



HAL
open science

Influence of urban pollution on the production of organic particulate matter from isoprene epoxydiols in central Amazonia

Suzane S de Sá, Brett B Palm, Pedro Campuzano-Jost, Douglas A Day, Matthew K Newburn, Weiwei Hu, Gabriel Isaacman-Vanwertz, Lindsay D Yee, Ryan Thalman, Joel Brito, et al.

► To cite this version:

Suzane S de Sá, Brett B Palm, Pedro Campuzano-Jost, Douglas A Day, Matthew K Newburn, et al.. Influence of urban pollution on the production of organic particulate matter from isoprene epoxydiols in central Amazonia. *Atmospheric Chemistry and Physics*, 2017, 17 (11), pp.6611 - 6629. 10.5194/acp-17-6611-2017. hal-01836085

HAL Id: hal-01836085

<https://uca.hal.science/hal-01836085v1>

Submitted on 12 Jul 2018

HAL is a multi-disciplinary open access archive for the deposit and dissemination of scientific research documents, whether they are published or not. The documents may come from teaching and research institutions in France or abroad, or from public or private research centers.

L'archive ouverte pluridisciplinaire **HAL**, est destinée au dépôt et à la diffusion de documents scientifiques de niveau recherche, publiés ou non, émanant des établissements d'enseignement et de recherche français ou étrangers, des laboratoires publics ou privés.



Influence of urban pollution on the production of organic particulate matter from isoprene epoxydiols in central Amazonia

Suzane S. de Sá¹, Brett B. Palm², Pedro Campuzano-Jost², Douglas A. Day², Matthew K. Newburn³, Weiwei Hu², Gabriel Isaacman-VanWertz^{4,a}, Lindsay D. Yee⁴, Ryan Thalman⁵, Joel Brito^{6,b}, Samara Carbone⁶, Paulo Artaxo⁶, Allen H. Goldstein⁴, Antonio O. Manzi⁷, Rodrigo A. F. Souza⁸, Fan Mei⁹, John E. Shilling^{3,9}, Stephen R. Springston⁵, Jian Wang⁵, Jason D. Surratt¹⁰, M. Lizabeth Alexander³, Jose L. Jimenez², and Scot T. Martin^{1,11}

¹School of Engineering and Applied Sciences, Harvard University, Cambridge, Massachusetts, USA

²Department of Chemistry & Biochemistry and Cooperative Institute for Research in Environmental Sciences, University of Colorado, Boulder, Colorado, USA

³Environmental Molecular Sciences Laboratory, Pacific Northwest National Laboratory, Richland, Washington, USA

⁴Dept. of Environmental Science, Policy, and Management, University of California, Berkeley, California, USA

⁵Brookhaven National Laboratory, Upton, New York, USA

⁶Departamento de Física Aplicada, Universidade de São Paulo, São Paulo, Brazil

⁷Instituto Nacional de Pesquisas da Amazonia, Manaus, Amazonas, Brazil

⁸Escola Superior de Tecnologia, Universidade do Estado do Amazonas, Manaus, Amazonas, Brazil

⁹Atmospheric Sciences and Global Change Division, Pacific Northwest National Laboratory, Richland, WA, USA

¹⁰Department of Environmental Sciences and Engineering, Gillings School of Global Public Health, The University of North Carolina at Chapel Hill, Chapel Hill, North Carolina, USA

¹¹Department of Earth and Planetary Sciences, Harvard University, Cambridge, Massachusetts, USA

^anow at: Massachusetts Institute of Technology, Cambridge, Massachusetts, USA

^bnow at: Laboratory for Meteorological Physics (LaMP), University Blaise Pascal, Aubière, France

Correspondence to: Scot T. Martin (scot_martin@harvard.edu)

Received: 16 November 2016 – Discussion started: 13 December 2016

Revised: 26 April 2017 – Accepted: 28 April 2017 – Published: 6 June 2017

Abstract. The atmospheric chemistry of isoprene contributes to the production of a substantial mass fraction of the particulate matter (PM) over tropical forests. Isoprene epoxydiols (IEPOX) produced in the gas phase by the oxidation of isoprene under HO₂-dominant conditions are subsequently taken up by particles, thereby leading to production of secondary organic PM. The present study investigates possible perturbations to this pathway by urban pollution. The measurement site in central Amazonia was located 4 to 6 h downwind of Manaus, Brazil. Measurements took place from February through March 2014 of the wet season, as part of the GoAmazon2014/5 experiment. Mass spectra of organic PM collected with an Aerodyne Aerosol Mass Spectrometer were analyzed by positive-matrix factorization. One resolved statistical factor (“IEPOX-SOA factor”) was associated with PM production by the IEPOX pathway. The IEPOX-SOA

factor loadings correlated with independently measured mass concentrations of tracers of IEPOX-derived PM, namely C₅-alkene triols and 2-methyltetrols ($R = 0.96$ and 0.78 , respectively). The factor loading, as well as the ratio f of the loading to organic PM mass concentration, decreased under polluted compared to background conditions. For an increase in NO_y concentration from 0.5 to 2 ppb, the factor loading and f decreased by two to three fold. Overall, sulfate concentration explained 37 % of the variability in the factor loading. After segregation of factor loading into subsets based on NO_y concentration, the sulfate concentration explained up to 75 % of the variability. Considering both factors, the data sets show that the suppressing effects of increased NO concentrations dominated over the enhancing effects of higher sulfate concentrations. The pollution from Manaus elevated NO_y concentrations more significantly than sulfate concen-

trations relative to background conditions. In this light, increased emissions of nitrogen oxides, as anticipated for some scenarios of Amazonian economic development, could significantly alter pathways of PM production that presently prevail over the tropical forest, implying changes to air quality and regional climate.

1 Introduction

Organic compounds comprise up to 90 % of the mass concentration of submicron organic particulate matter (PM) over tropical forests (Kanakidou et al., 2005). Submicron PM has adverse effects on human health (Nel, 2005; Pope III and Dockery, 2006) and influences air quality and climate by scattering radiation and acting as cloud condensation nuclei (Ramanathan et al., 2001; Kaufman et al., 2002). A significant fraction of the submicron organic material originates from secondary processes, mainly by the atmospheric oxidation of volatile organic compounds (VOCs) emitted as part of natural and human activities (Zhang et al., 2007; Hallquist et al., 2009; Jimenez et al., 2009). The particle life cycle over Amazonia is in particular strongly influenced by secondary processes that produce organic PM (Martin et al., 2010a; Pöschl et al., 2010). Biogenic emissions from tropical forests are high, and environmental conditions favor photooxidation reactions. The reactive chemistry and the relative importance of pathways leading to PM production can be strongly guided by regulating species, such as sulfate and nitric oxide (NO) (Surratt et al., 2007a; Worton et al., 2013; Liu et al., 2016a). The concentrations of these species depend on their background occurrence, pollution sources, and the relative mix of background and polluted air masses.

Over tropical forests such as Amazonia, the atmospheric chemistry of isoprene produces a substantial fraction of the submicron organic PM (Chen et al., 2009, 2015; Robinson et al., 2011; Isaacman-VanWertz et al., 2016). Isoprene (2-methyl-1,3-butadiene, C_5H_8) is the non-methane VOC most abundantly emitted by tropical forests (Guenther et al., 2012), and isoprene epoxydiols (IEPOX) have been identified as important intermediates in the production of PM from isoprene (Paulot et al., 2009; Surratt et al., 2010; Lin et al., 2012). A chemical sequence for the production of IEPOX-derived PM from the photooxidation of isoprene in the atmosphere is represented in Fig. 1. The sequence is initiated when isoprene peroxy radicals (ISOPOO) are produced in the gas phase by reactions between isoprene and photochemically generated hydroxyl radicals (OH). The reactive fate of the ISOPOO radicals can differ under background compared to polluted conditions (Surratt et al., 2010; Crouse et al., 2011; Worton et al., 2013).

Under background conditions, meaning that HO_2 pathways are favorable in the absence of extensive NO pollution (Wennberg, 2013; Liu et al., 2016a), the ISOPOO rad-

icals continue in large part through the series of species highlighted in yellow in Fig. 1. Through HO_x -facilitated reaction steps, the ISOPOO radicals produce hydroperoxides (ISOPOOH) as major first-generation products and subsequently IEPOX as major second-generation products (Carlton et al., 2009; Paulot et al., 2009; Liu et al., 2013, 2016a; St. Clair et al., 2015). Some of the produced IEPOX undergoes reactive uptake to particles, as facilitated by hydronium ions at the surface (Surratt et al., 2007a; Lin et al., 2012; Gaston et al., 2014; Kuwata et al., 2015; Lewandowski et al., 2015). This chemical sequence can contribute a significant fraction of submicron PM mass concentration over tropical forests (Claeys et al., 2004; Hu et al., 2015). Laboratory studies indicate that about half of the PM produced by isoprene photooxidation under HO_2 -dominant conditions in the presence of acidic sulfate particles is associated with IEPOX production and uptake (Liu et al., 2015). Interaction of IEPOX with cloud waters warrants investigation (Lim et al., 2005; Ervens et al., 2011; Budisulistiorini et al., 2015; Chen et al., 2015). In addition to IEPOX pathways, laboratory studies suggest that multifunctional hydroperoxides produced in the gas phase can contribute to isoprene-derived PM production (Krechmer et al., 2015; Liu et al., 2016b; Riva et al., 2016b).

After reactive uptake of IEPOX, particle-phase reactions can produce several different families of species. These species are collectively labeled “IEPOX-derived PM” and represent a subset of the ambient organic PM, as labeled in Fig. 1. The presence of 2-methyltetrols, C_5 -alkene triols, 3-methyltetrahydrofuran-3,4-diols, organosulfates, and related oligomers in ambient PM is an indicator of PM production by IEPOX uptake under atmospheric conditions (Claeys et al., 2004; Surratt et al., 2006, 2007b, 2010; Robinson et al., 2011; Lin et al., 2012, 2014). Even though these species may differ in some cases from the actual compounds in the atmospheric PM due to thermal decomposition during analysis (Lopez-Hilfiker et al., 2016), they serve as chemical tracers for the atmospheric concentration of IEPOX-derived PM (Hu et al., 2015; Isaacman-VanWertz et al., 2016). The analytical methods highlighted in Fig. 1, including that of retrieving an “IEPOX-SOA factor” from mass spectral analysis used herein, can lead to over- and underestimated IEPOX-derived PM concentrations. This uncertainty is represented in the figure by the brown dashed lines that approximately but not exactly correspond to IEPOX-derived PM.

Under polluted conditions, the reactive sequence of isoprene and ultimately PM production can become significantly altered (Fig. 1). NO concentrations can be sufficiently high that ISOPOO radicals react almost entirely with NO in place of HO_2 , thereby largely producing methacrolein (MACR) and methyl vinyl ketone (MVK) in place of ISOPOOH (Liu et al., 2016a). As a result, IEPOX production can be greatly decreased, ultimately reducing PM production by IEPOX pathways. A minor channel along the NO pathway can still produce IEPOX, although much less efficiently (Jacobs et al., 2014). Under NO-dominant conditions,

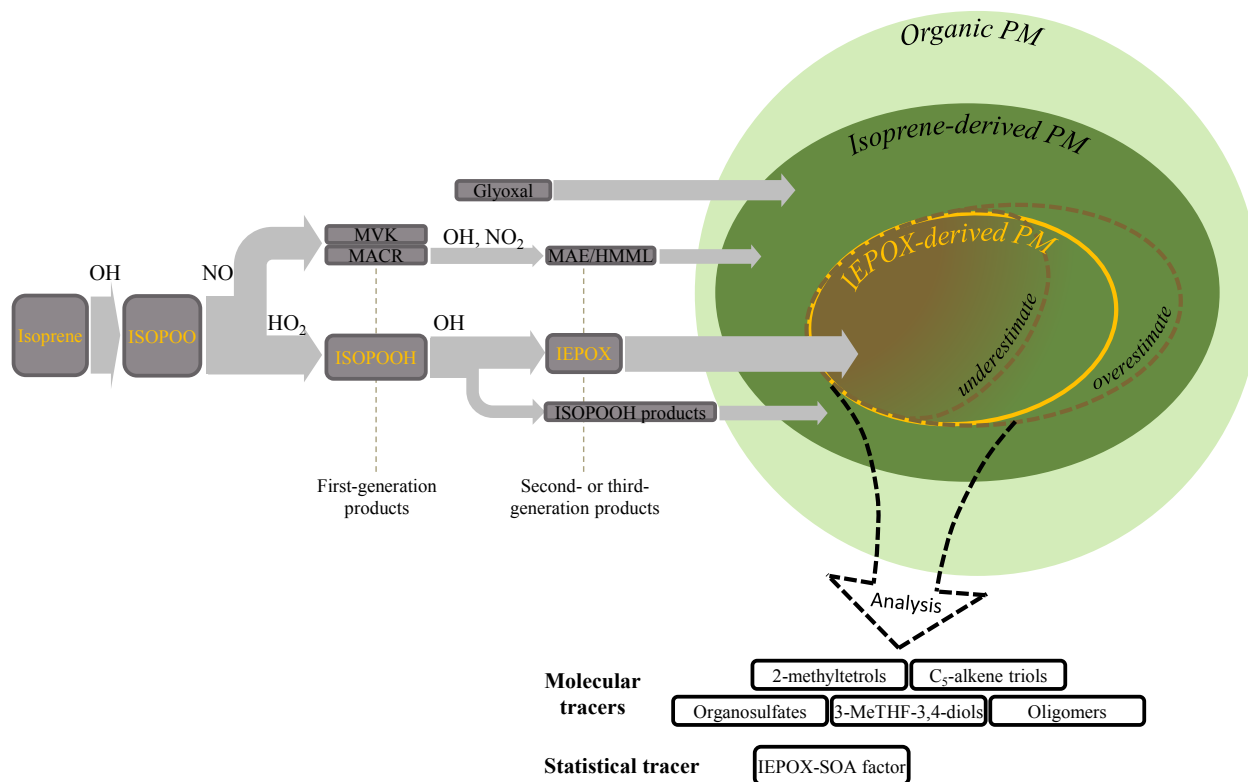


Figure 1. Schematic diagram for the production of PM derived from isoprene epoxydiols (IEPOX) produced during the photooxidation of isoprene. Organic peroxy radicals (ISOPOO), produced by OH attack and O_2 addition to isoprene, are scavenged along NO or HO_2 pathways. By the HO_2 pathway, organic hydroperoxides (ISOPOOH) are first-generation products that react with additional OH to produce IEPOX. The IEPOX species undergo reactive uptake into particles, ultimately producing IEPOX-derived particulate matter. Arrow thickness qualitatively illustrates the relative importance (i.e., mass flux) of a reaction channel under background conditions. Gray and green background colors indicate species in the gas and particle phases, respectively. The light-green disk represents the total organic PM. Within that disk, the contribution by isoprene-derived PM, including compounds produced both IEPOX and non-IEPOX pathways, is represented by the dark-green oval. Inside that oval, the contribution by IEPOX-derived PM is represented by the yellow oval region. The color gradient between brown and dark green illustrates the chemical modification of the IEPOX-derived PM over time. The large dashed black arrow represents the analytical methods that use different types of molecular and statistical tracers (listed in the boxes) to quantify the IEPOX-derived PM mass concentrations. For simplicity, the figure omits the many routes leading to the production of glyoxal (Fu et al., 2008), possible ISOPOO isomerization when NO and HO_2 concentrations are sufficiently low (Crouse et al., 2011; Liu et al., 2016a), second-generation production of peroxyacetic nitric anhydride (Lin et al., 2013; Nguyen et al., 2015), and particle water and other inorganic components. 3-methyltetrahydrofuran-3,4-diols are abbreviated as 3-MeTHF-3,4-diols. Other abbreviations are provided in the main text.

alternative pathways of PM production not involving IEPOX can become active, though in lower yields. MACR can be oxidized to produce peroxyacetic nitric anhydride (MPAN), which is a precursor to methacrylic acid epoxide (MAE) and hydroxymethylmethyl- α -lactone (HMML), and these compounds can undergo reactive uptake to produce PM (Kjaergaard et al., 2012; Lin et al., 2013; Worton et al., 2013; Nguyen et al., 2015). Glyoxal produced from isoprene oxidation can contribute to PM production (Volkamer et al., 2007; Ervens and Volkamer, 2010; McNeill et al., 2012; Marais et al., 2016).

Another possible mechanism affecting PM production by IEPOX uptake under polluted conditions is altered particle composition, especially particle acidity, largely driven

by sulfate. Laboratory studies show that IEPOX uptake increases with increasing acidity (Gaston et al., 2014; Kuwata et al., 2015; Liu et al., 2015). A proposed reaction during uptake is the acid-catalyzed ring opening of the IEPOX molecule (Surratt et al., 2010). The subsequent particle-phase reactions include the addition of available nucleophiles, such as water to produce tetrols or sulfate to produce organosulfates as well as their oligomers (Surratt et al., 2010; Lin et al., 2014; Nguyen et al., 2014). In support of this proposed mechanism, analyses by positive-matrix factorization (PMF) of mass spectra collected in the southeastern USA identified PMF factors associated with IEPOX-derived PM, and these factors correlated positively with sulfate mass concentrations (Budisulistiorini et al., 2013; Hu et al., 2015;

Xu et al., 2015). In short, different regimes of $\text{NO}:\text{HO}_2$ concentration ratios and different possible PM compositions between polluted and background conditions can lead to different product distributions and different production rates of IEPOX-derived PM.

The extent to which pollution may shift the production pathways of IEPOX-derived PM over tropical forests remains to be elucidated. The study described herein is based on data sets collected in the wet season downwind of Manaus, Brazil, during the Observations and Modeling of the Green Ocean Amazon (GoAmazon2014/5) experiment (Martin et al., 2016a). The research site was influenced at times and to variable extents by the pollution outflow from the Manaus metropolitan area. Compared to the background environment in Amazonia, the Manaus plume had high number concentrations of particles and enhanced concentrations of pollutants, including oxides of nitrogen and sulfate (Kuhn et al., 2010; Martin et al., 2016a). The reactive gas-phase chemistry was strongly guided by the relative mix of background and polluted air masses (Trebs et al., 2012; Liu et al., 2016a). The analysis herein focuses on how the pollution perturbed IEPOX-derived PM production relative to background conditions.

2 Methodology

Data sets were collected at the “T3” site (3.2133°S , 60.5987°W) located 70 km to the west of Manaus, Brazil, in central Amazonia (Martin et al., 2016a). The site was situated in a pasture ($2.5\text{ km} \times 2\text{ km}$) surrounded by forest. The analysis herein focuses on data sets collected during the wet season period of 1 February to 31 March 2014, corresponding to the first Intensive Operating Period (IOP1) of the GoAmazon2014/5 experiment.

A High-Resolution Time-of-Flight Aerosol Mass Spectrometer (HR-ToF-AMS, hereafter AMS; Aerodyne, Inc., Billerica, Massachusetts, USA) recorded the primary data set of this study. The AMS provided quantitative bulk characterization of the atmospheric PM. The design principles and capabilities of this instrument are described in the literature (DeCarlo et al., 2006; Canagaratna et al., 2007). The instrument was housed within a temperature-controlled research container, and the inlet to the instrument sampled from 5 m above ground level. Detailed aspects of AMS operation are presented in the Supplement (Sect. S1). In brief, ambient measurements were obtained every other 4 min. Organic, sulfate, ammonium, nitrate, and chloride PM mass concentrations were obtained from “V-mode” data. The choice of ions to fit was aided by the “W-mode” data, which were collected for 1 day every 5 days. Data analysis was performed using SQUIRREL (1.56D) and PIKA (1.14G) of the AMS software suite.

Positive-matrix factorization was applied to the time series of the organic component of the high-resolution mass spectra (Ulbrich et al., 2009). The present study focuses on one of the resolved statistical factors, referred to as the IEPOX-SOA factor (Hu et al., 2015). Diagnostics of the PMF analysis, especially as related to the resolved IEPOX-SOA factor, are presented in the Supplement (Sect. S2). A separate account is forthcoming to present the other PMF factors (de Sá, 2017). Herein, “factor profile” and “factor loading” refer to the mathematical products of the multivariate statistical analysis, whereas “mass spectrum” and “mass concentration” refer to measurements.

Complementary to the AMS data sets, mass concentrations of molecular and tracer organic species were measured using a semivolatile thermal desorption aerosol gas chromatograph (SV-TAG) at a time resolution of 1 h. The instrument collected gas and particle samples, followed by thermal desorption, derivatization, and gas chromatography coupled to mass spectrometry (Isaacman et al., 2014). A summary of operational details for GoAmazon2014/5 is presented in the Supplement (Sect. S1), and the main account is presented in Isaacman-VanWertz et al. (2016).

Additional data sets used in the analysis were collected at the T3 site by instruments housed in the research container of the Mobile Aerosol Observing System (MAOS) of the ARM Climate Research Facility (ACRF) operated by the USA Department of Energy (Mather and Voyles, 2013; Martin et al., 2016a). A temperature-controlled inlet was mounted at 10 m above ground level. Measurements of nitrogen oxides were made using a chemiluminescence-based instrument (Air Quality Design). The measured odd-nitrogen family “ NO_y ”, meaning NO_x plus reservoir species, included NO , NO_2 , HNO_3 , organonitrates, particle nitrate, and peroxyacetyl nitrates. Further details of the NO_y measurements are presented in the Supplement (Sect. S1). Ozone concentrations were measured by an ozone analyzer (Thermo Fisher, model 49i). Particle number concentrations were measured by a condensation particle counter (TSI, model 3772). Meteorological variables provided by the ARM Mobile Facility (AMF-1), which was also part of the ACRF, included wind direction, solar irradiance, and precipitation rate. Measurements of NO_y and particle number concentration onboard the G-1 aircraft of the ARM Aerial Facility (AAF) were also used in the analysis (Schmid et al., 2014; Martin et al., 2016a).

3 Results and discussion

The organization of the presentation herein is as follows. The factor profile obtained from AMS PMF analysis is discussed (Sect. 3.1), a case study comparing factor loading under background to polluted conditions is presented (Sect. 3.2), the roles of sulfate (Sect. 3.3) and nitric oxide (Sect. 3.4) in affecting factor loading are explored, and the influence of

NO on production and loss processes of IEPOX-derived PM is considered (Sect. 3.5).

3.1 Statistical IEPOX-SOA factor

Positive-matrix factorization was carried out on the time series of AMS organic mass spectra. One statistical factor had a similar profile of peak intensities as the IEPOX-SOA factor identified in other studies (Fig. S1 in the Supplement) (Robinson et al., 2011; Slowik et al., 2011; Budisulistiorini et al., 2013, 2015; Chen et al., 2015; Xu et al., 2015). The Pearson correlation coefficient R between this factor and the one obtained in the 2008 wet season in central Amazonia as part of the AMAZE-08 experiment was 0.99 (Chen et al., 2015). The ratio f of the factor loading to the mass concentration of submicron organic PM for the present study was 0.17 ± 0.09 (mean \pm standard deviation). The IEPOX-SOA factor has been identified previously over the maritime tropical forest of Borneo ($f = 0.23$) (Robinson et al., 2011), in a rural area in Canada 70 km north of Toronto ($f = 0.17$) (Slowik et al., 2011), across several locations in the southeastern USA in summertime ($f = 0.17$ to 0.41) (Budisulistiorini et al., 2013, 2015, 2016; Hu et al., 2015; Xu et al., 2015; Marais et al., 2016), and in AMAZE-08 ($f = 0.34$) (Chen et al., 2015). A further review of the ubiquity and characteristics of the IEPOX-SOA factor is presented in Hu et al. (2015).

The IEPOX-SOA factor reported herein had prominent peaks at m/z 53.04 and m/z 82.04 (Fig. S1). The ion at m/z 82.04, corresponding to $C_5H_6O^+$, has been attributed to 3-methylfuran (3-MF). The thermal degradation of isoprene-derived PM upon mass spectral analysis was suggested as the source of 3-MF (Robinson et al., 2011). Lin et al. (2012) proposed that sequential dehydrations upon mass spectral analysis of 3-methyltetrahydrofuran-3,4-diols, which are an identified component of IEPOX-derived PM, can produce 3-MF. Other IEPOX-derived species as well as non-IEPOX species might also contribute to the production of $C_5H_6O^+$ ions (Surratt et al., 2010; Hu et al., 2015; Liu et al., 2016c).

Laboratory studies show that a mass spectrum that is a pattern of peak intensities similar to that of the IEPOX-SOA factor is produced by the uptake of IEPOX into aqueous acidic sulfate particles as well as by the photooxidation of isoprene under HO_2 -dominant conditions in the presence of acidic sulfate particles (Budisulistiorini et al., 2013; Nguyen et al., 2014; Kuwata et al., 2015; Liu et al., 2015). The possibility of similar uptake by a broader range of liquid media remains to be fully tested, such as other acidic solutions as well as cloud waters. Compared to the laboratory spectra of Liu et al. (2015), representing about 4 h of OH exposure at atmospheric concentrations (1.7×10^6 molec cm^{-3}), the main difference was the relative intensity of the m/z 44 peak. For the IEPOX-SOA factor of the present study, this peak was 4 times more intense (Fig. S1), suggesting that the atmospheric PM was more oxidized. Hu et al. (2016) showed that hetero-

geneous aging of IEPOX-SOA can result in increased relative signal at m/z 44.

By contrast, laboratory studies show that a significantly different mass spectrum from that of the IEPOX-SOA factor is obtained for PM produced from isoprene photooxidation in the absence of aqueous particles (Krechmer et al., 2015; Kuwata et al., 2015). Under these conditions, chemical pathways other than IEPOX uptake into a liquid medium appear to be active, such as the condensation of low-volatility, multifunctional compounds produced by additional oxidation of ISOPOOH (Krechmer et al., 2015; Liu et al., 2016b; Riva et al., 2016b). This non-IEPOX pathway, however, is not expected to contribute a large fraction of the produced PM during the study period because of the high relative humidity conditions in Amazonia and the prevalence of liquid particles for the prevailing atmospheric conditions (Bateman et al., 2016; de Sá, 2017).

The SV-TAG measurements of the concentrations of C_5 -alkene triols and 2-methyltetrols support the interpretation of the IEPOX-SOA factor as an indicator that PM was being produced, at least in significant part, from the reactive uptake of IEPOX (Claeys et al., 2004; Wang et al., 2005; Surratt et al., 2010). The factor loading strongly correlated with the concentrations of C_5 -alkene triols ($R = 0.96$) and 2-methyltetrols ($R = 0.78$) (Fig. 2). These species have been associated with the IEPOX reaction pathway in several laboratory studies (Surratt et al., 2010; Riedel et al., 2016). The R value with respect to C_5 -alkene triols was independent of the f_{peak} value of the PMF solution, demonstrating the robustness of the relative time trend of factor loading even though the factor profile and absolute loadings changed across f_{peak} values (Fig. S2d).

The loading of the IEPOX-SOA factor may be an overestimate or an underestimate of the atmospheric concentration of the IEPOX-derived PM (Supplement, Sect. S2). The IEPOX-SOA factor can be understood as the net result of (i) produced IEPOX-derived PM, (ii) minus that portion of the carbon that gets further oxidized and mixed into other PMF factors, and (iii) plus that portion of non-IEPOX-derived PM that gives rise to a similar AMS mass spectral pattern as the IEPOX-derived PM (Supplement, Sect. S2). Processes of type ii contribute to underestimates and processes of type iii lead to overestimates when using IEPOX-SOA factor loading as a surrogate for IEPOX-derived PM concentration. These uncertainties are qualitatively represented in Fig. 1 by the brown dashed lines that enclose the fraction of particle material statistically captured by the factor analysis. The further analysis herein is based on using the loading of the IEPOX-SOA factor as a scalar proxy for the mass concentration of IEPOX-derived PM in a sampled air mass.

3.2 Background compared to polluted conditions

Under background conditions in the wet season, remote areas of the Amazon forest constitute one of the least-polluted

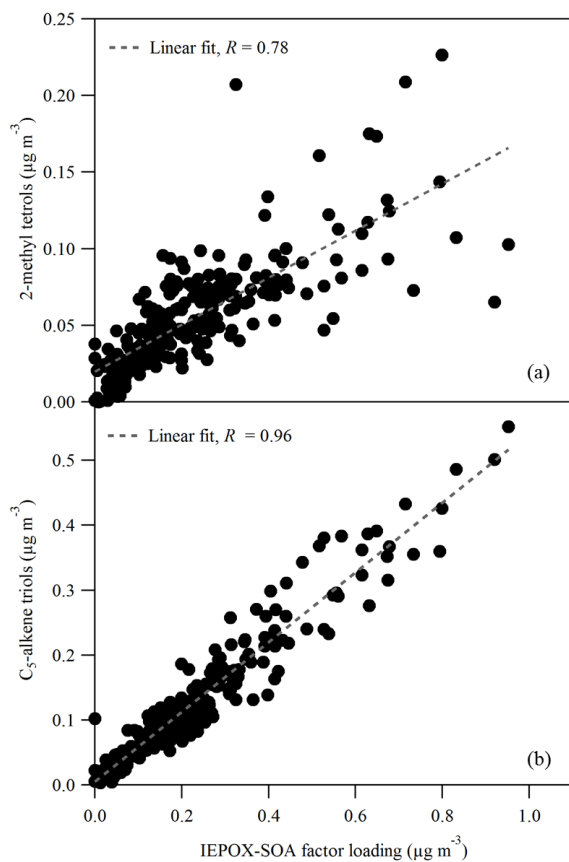


Figure 2. Scatter plot of the loading of the IEPOX-SOA factor derived from analysis of the AMS data set and the mass concentrations of C_5 -alkene triols and 2-methyltetrols measured by SV-TAG. All data collected during the IOP1 period are included, meaning that the plotted data are not limited to afternoon time periods.

continental regions on Earth (Martin et al., 2010a). Nitric oxide concentrations characteristic of central Amazonia range from 20 to 70 ppt (Torres and Buchan, 1988; Bakwin et al., 1990; Levine et al., 2015). Daytime maximum ozone concentrations are 10 to 15 ppb (Rummel et al., 2007). Sulfate mass concentrations associated with in-basin processes are on average $< 0.1 \mu\text{g m}^{-3}$, and total background sulfate concentrations contributed by in- and out-of-basin processes rarely exceed $0.5 \mu\text{g m}^{-3}$ (Andreae et al., 1990; Chen et al., 2009).

In the wet season, Manaus emissions were the most important anthropogenic influence on observations at the T3 research site (Martin et al., 2017). The afternoons of 3 and 13 March 2014 are presented herein as representative cases of background and polluted conditions, respectively. Both days were sunny, and major precipitation events were absent. Particle number concentrations measured onboard the G-1 aircraft within the atmospheric boundary layer show the position of the pollution plume on these two afternoons (Fig. 3). NO_y concentrations measured during the same flight are shown in Fig. S3. The visualization in Fig. 3 shows

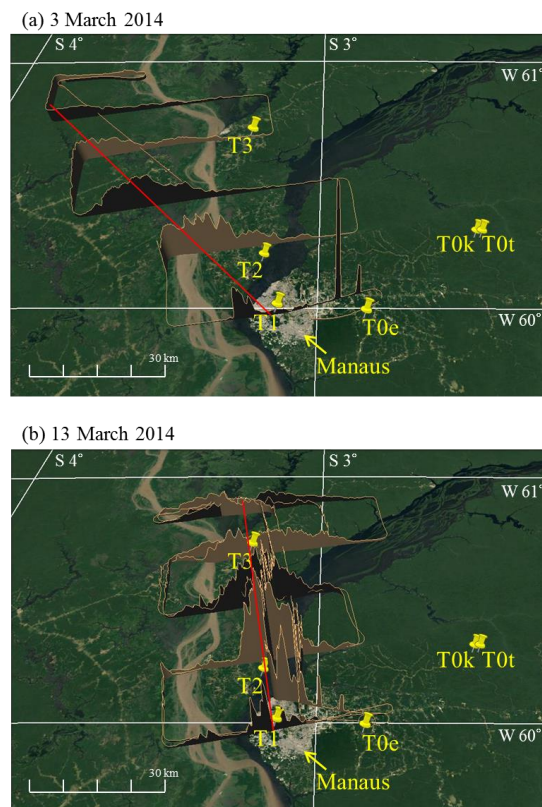


Figure 3. Visualization of the Manaus pollution plume by plotting particle number concentrations in the vertical axis. Observations took place on flights from late morning to early afternoon on (a) 3 March 2014, 17:45–19:26 UTC, and (b) 13 March 2014, 14:14–17:21 UTC. Local time is UTC – 4 h. The red lines guide the eye through the central axis of the plume. The direction and extent of the plume was observed by the G-1 aircraft within the atmospheric boundary layer downwind of Manaus. Measured particle number concentrations are plotted on a vertical axis on top of an image of land cover in the horizontal plane. Particle concentrations in the center of the plume ranged from 10 000 to 25 000 cm^{-3} nearby Manaus. Yellow pins indicate the locations of some of the GoAmazon2014/5 research sites, including T3 (Martin et al., 2016a).

that on 3 March the Manaus plume passed south of the T3 site. By comparison, on 13 March the central portion of the plume passed over T3. Aircraft-based observations to track the Manaus plume were available for 16 afternoons of the 2-month study period.

Measurements at ground level at the T3 site are plotted in Fig. 4 for the afternoons of 3 March (left panel) and 13 March (right panel). Based on wind speeds, the research site was 4 to 6 h downwind of Manaus (Martin et al., 2016a). Anthropogenic-biogenic interactions affecting the production of IEPOX-derived PM were driven in large part by atmospheric photochemistry at daybreak. Morning urban emissions followed by atmospheric processing arrived at the T3 site during the local afternoon. The afternoon period, in ad-

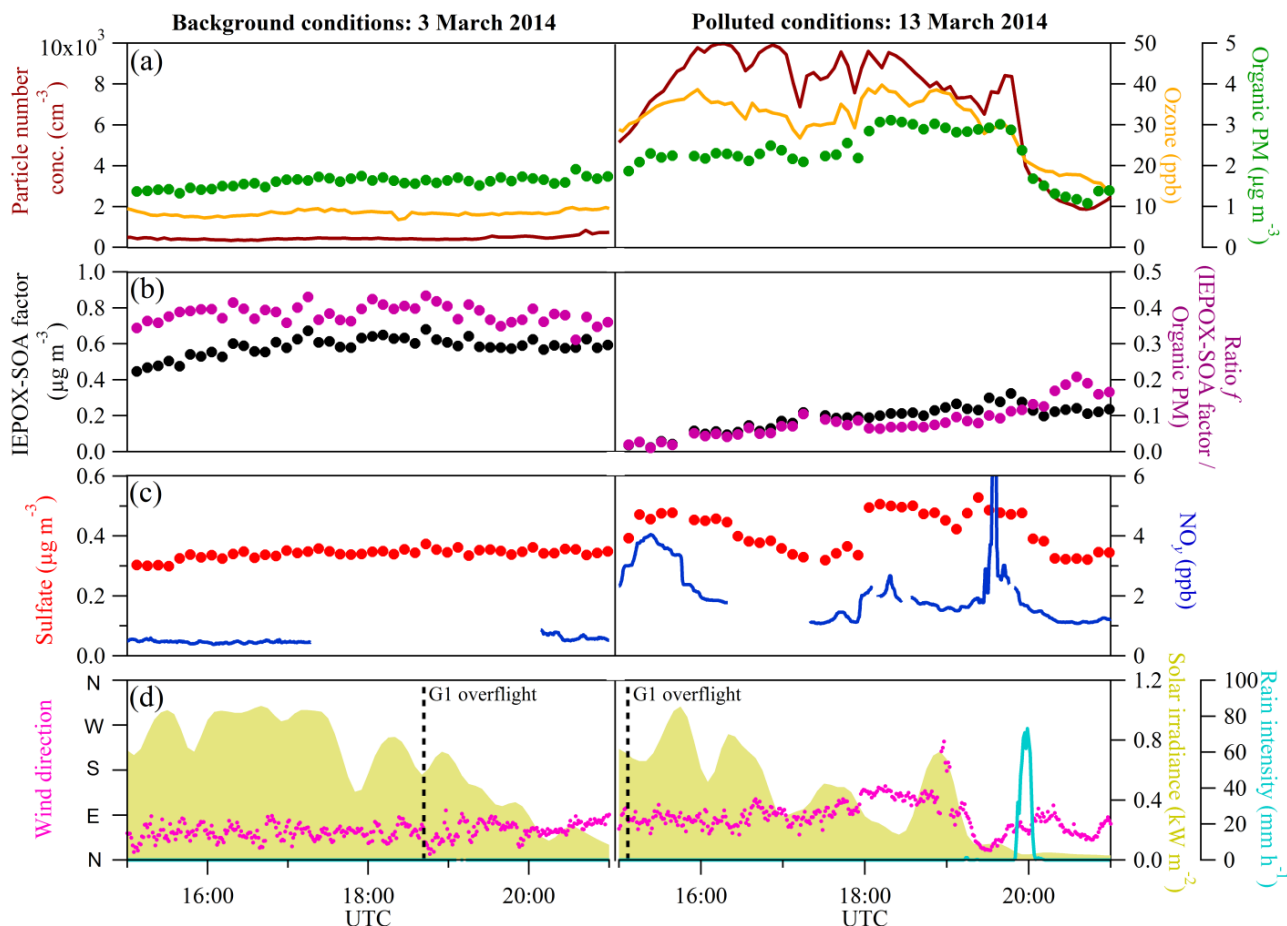


Figure 4. Case studies of (left) background and (right) polluted air masses passing over T3 on afternoons of 3 and 13 March 2014. (a) Ozone, particle number, and organic mass concentration. (b) IEPOX-SOA factor loading and the ratio f of the factor loading to the organic PM concentration. (c) Sulfate and NO_y concentrations. (d) Wind direction, rain intensity, and solar irradiance. Local time is UTC – 4 h. Time points of overflights at 500 m by the G-1 research aircraft are marked by the dashed line (Martin et al., 2016a).

dition to the connection to the Manaus plume, was also characterized by reduced variability in other possible confounding variables, such as temperature, radiation, and relative humidity. Figure 4 shows that on the afternoon of 3 March ozone concentrations were below 10 ppb, particle number concentrations were below 1000 cm^{-3} , NO_y concentrations were less than 1 ppb, and sulfate concentrations were 0.3 to $0.4 \mu\text{g m}^{-3}$. Species concentrations were stable throughout the afternoon. On 13 March, ozone concentrations exceeded 30 ppb for most of the afternoon, particle concentrations reached $10\,000 \text{ cm}^{-3}$, NO_y concentrations consistently exceeded 1 ppb, and sulfate concentrations were 0.3 to $0.6 \mu\text{g m}^{-3}$. Concentrations fluctuated markedly throughout the afternoon on 13 March, reflecting different levels of pollution influence in the air passing over the T3 site during that period.

Elevated concentrations of ozone, particle number, and NO_y were reliable markers of pollution influence over the course of the study period (Supplement, Sect. S3). Pollution

was associated with stronger relative enhancements in NO_y concentrations than in sulfate concentrations (Sect. 3.3 and 3.4). With respect to the IEPOX-SOA factor, Fig. 4 shows that the absolute and relative loadings decreased for the polluted compared to background conditions. Relative loadings are expressed by the ratio f of IEPOX-SOA factor loading to the organic PM mass concentration. Decreased absolute and relative factor loadings under polluted conditions, presented in Fig. 4 as a case study, also characterized the data sets of the entire study period. Other examples are presented in the Supplement (Fig. S4).

3.3 Sulfate as a driver of IEPOX-derived PM production

A scatter plot between sulfate mass concentrations and IEPOX-SOA factor loadings for all afternoon periods is shown in Fig. 5a. Background and polluted conditions are represented in the data set. For further visualization, the data

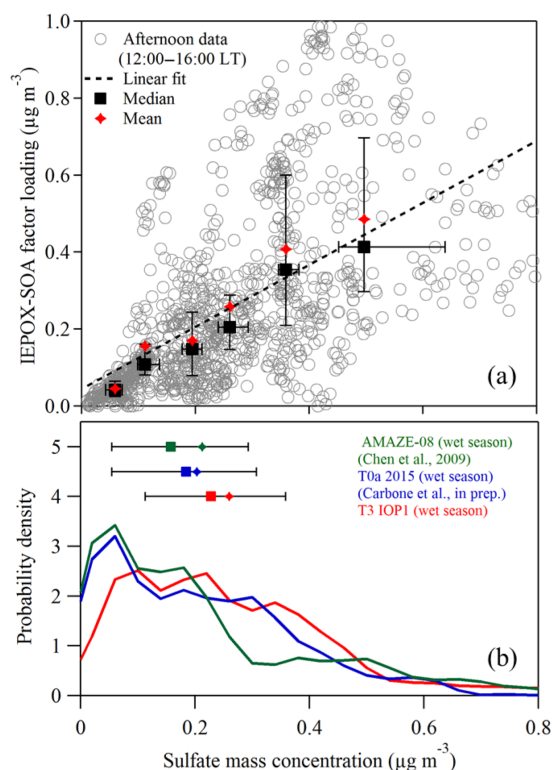


Figure 5. (a) Scatter plot of sulfate mass concentration and IEPOX-SOA factor loading. A least-squares linear fit is represented by the dashed line ($R^2 = 0.37$). The data set was collected into six subsets based on sulfate concentration to calculate statistics. Medians (squares) and means (diamonds) of each subset are plotted. Whiskers on the medians represent the interquartile ranges. (b) Probability density function of sulfate mass concentration at the background site T0t (TT34) north of Manaus in the wet season of 2008 (Chen et al., 2009; Martin et al., 2010b, 2016b), at the background site T0a (ATTO) northeast of Manaus in the wet season of 2015 (Andreae et al., 2015), and at T3 during the wet season of 2014 (IOP1). The plotted data sets were recorded during local afternoons (12:00–16:00 local time; 16:00–20:00 UTC). Means (diamonds), medians (squares), and interquartile range (whiskers) are shown for the probability density functions.

set was organized into six subsets based on sulfate concentration. The medians and the means of the subsets are plotted in the figure. The visualization shows that sulfate concentration served as a first-order predictor of the IEPOX-SOA factor loading in central Amazonia in the wet season. The explanation can be a combination of increased acidity, greater reaction volume including by enhanced hygroscopic growth, and possibly a nucleophilic role for sulfate (Xu et al., 2015; Marais et al., 2016). An analysis of the relative importance of each is out of the scope of the present study (Supplement, Sect. S4).

For Fig. 5a, the coefficient R^2 of determination between sulfate mass concentration and factor loading was 0.37, meaning that 37 % of the variance of the IEPOX-SOA fac-

tor loading was explained by sulfate mass concentration. As a point of comparison, R^2 varied between 0.4 and 0.6 for observations in the southeastern USA, which seasonally is a region of high isoprene emissions (Budisulistiorini et al., 2013, 2015; Hu et al., 2015; Xu et al., 2015). A chemical transport model that predicted IEPOX-derived PM mass concentration for the southeastern USA obtained R^2 of 0.4 for the relationship to predicted sulfate mass concentration (Marais et al., 2016). The model attributed the correlation to the acidity and particle volume provided by sulfate, both of which favored IEPOX uptake. Central Amazonia and the southeastern USA differ considerably in terms of meteorology, chemistry, and levels of regional pollution, yet they have in common an important role of sulfate concentration as a predictor of IEPOX-derived PM concentration, even as the sulfate concentrations themselves differ by an order of magnitude. Sulfate concentrations typically had an interquartile range of $[1.5, 3.0] \mu\text{g m}^{-3}$ in the studies in the southeastern USA, which can be compared to a range of $[0.11, 0.36] \mu\text{g m}^{-3}$ under background conditions during the wet season in central Amazonia.

A key difference between the southeastern USA and central Amazonia is the role of sulfate concentration as a clear or ambiguous indicator, respectively, of urban influence. For the relatively low sulfate mass concentrations ($< 0.5 \mu\text{g m}^{-3}$) characteristic of the study period, background air in central Amazonia contributed significantly to the variability in sulfate concentration measured at the T3 site. Background concentrations of sulfate in Amazonia, distinguished from sulfate tied to the urban Manaus plume, originated from in-basin emissions of gas-phase precursors such as dimethyl sulfide (DMS) and hydrogen sulfide (H_2S) from the forest as well as from out-of-basin marine emissions from the Atlantic Ocean (Andreae et al., 1990; Chen et al., 2009; Martin et al., 2010a). In the wet season, biomass burning from Africa and to a lesser extent from South America also episodically contributed significantly to sulfate concentrations in the Manaus region. In addition, emissions from large cities on the eastern coast of Brazil were important at times when rare meteorological events shifted the northeasterlies typical of the wet season to easterlies (Martin et al., 2017). Manaus contributions to sulfate mass concentrations in an air mass were in addition to these various background sources.

The relative importance of Manaus contributions to the sulfate concentrations in the air masses that passed over T3 was assessed by comparison of the probability density function of sulfate concentration at T3 to those of sites upwind of Manaus (Fig. 5b). The distributions of the two upwind sites had a central tendency of 0.05 to $0.3 \mu\text{g m}^{-3}$, suggesting the range of natural concentrations, and a right-side skewness up to $0.6 \mu\text{g m}^{-3}$, suggesting the importance of episodic long-range transport (Chen et al., 2009). The figure shows that the distribution at T3 did not differ greatly from those of the upwind sites even though the air masses over T3 regularly transported Manaus pollution. The implication is that Man-

Table 1. Parameters associated with the NO_y groupings of Fig. 6. Listed are the NO_y concentrations and the parameters for least-squares linear fits to each group. R^2 represents the coefficient of determination.

Group	NO_y range (ppb)	Fit slope	Fit intercept	Fit R^2
1	> 0.66	2.16	−0.13	0.75
2	0.66–0.92	1.48	−0.04	0.64
3	0.92–1.55	0.78	0.06	0.24
4	1.55–2.45	0.71	−0.01	0.44
5	> 2.45	0.55	−0.02	0.62

aus sulfate sources, whether primary or secondary, had small contributions relative to background sources when averaged over time. In short, elevated sulfate concentrations on any one afternoon at the T3 site might have arisen because of elevated background concentrations on that day rather than the influence of the Manaus pollution plume. The implications are that (i) sulfate concentration was an ambiguous indicator of urban influence at the T3 site and (ii) increases in sulfate concentrations in pollution events were moderate relative to background concentrations.

3.4 NO as a modulator of IEPOX-derived PM production

In the transport from Manaus to the T3 research site, NO concentration was not conserved, in part because of reactions with ozone and organic peroxy radicals (Martin et al., 2017). In this case, the instantaneous NO concentrations measured at the T3 site did not directly provide information about the fate of ISOPOO radicals along the transport time of 4 to 6 h from Manaus to the T3 site. The collective contributions of NO , NO_2 , and their oxidation products were, however, reflected in measurements of NO_y concentrations at the T3 site. The NO_y family is expected to have a longer lifetime than the transport time from Manaus to the T3 site (Romer et al., 2016). The NO_y concentration measured at T3 therefore served as a surrogate for the integrated exposure of the air mass to NO chemistry between Manaus and T3 (Liu et al., 2016a).

Unlike the ambiguity associated with the sulfate concentration, an elevated NO_y concentration served as a clear indicator of anthropogenic influence in an air mass passing over the T3 site. For background conditions over the forest, NO_y originates from NO emitted from soils and other natural sources such as lightning (Bakwin et al., 1990; Jacob and Wofsy, 1990). The probability density function of NO_y concentration under background conditions in the wet season of the central Amazon basin is shown in Fig. 6b (Bakwin et al., 1990). The distribution for measurements at T3 is also shown. Relative to the narrow distribution around 0.5 ppb for background conditions, there is high-side skewness extend-

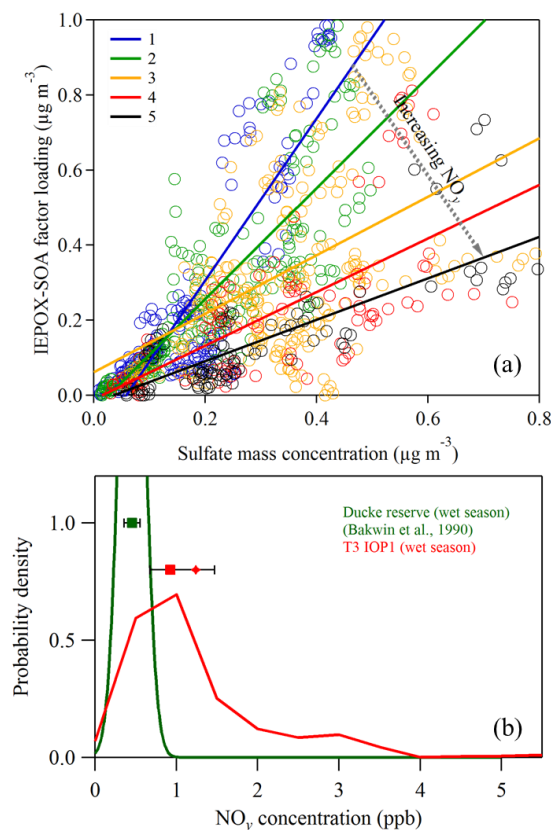


Figure 6. (a) Scatter plot of sulfate mass concentration and IEPOX-SOA factor loading for local afternoon (12:00–16:00 local time; 16:00–20:00 UTC). The data sets were collected into five subsets, colored and labeled 1 to 5, based on NO_y concentration. Table 1 presents the parameters of the five least-squares linear fits represented by the colored lines in the figure. (b) Probability density function of NO_y concentration at a background site nearby Manaus in the wet season of 1987 (Bakwin et al., 1990) and at T3 during the wet season of 2014 (IOP1) (afternoon data). Means (diamonds), medians (squares), and interquartile range (whiskers) are shown for the probability density functions. Additional analysis of (a) is presented in the Supplement (Sect. S5) related to Fig. S5.

ing up to 4 ppb for the T3 measurements, indicating the clear influence of Manaus emissions on NO_y concentrations.

NO_y concentration was incorporated into the analysis by segregation of the data set of Fig. 5a into five subsets (Supplement, Sect. S5). Linear fits to the NO_y -segregated data subsets are plotted in Fig. 6a. Each subset is represented by a different color. Parameter values of the associated fits are listed in Table 1. In conjunction with sulfate concentration, the visualization presented in Fig. 6a shows that NO_y concentration further explained the variability in IEPOX-SOA factor loadings. The R^2 values, representing the extent to which sulfate was able to explain variability in IEPOX-SOA factor loading once isolated for NO_y concentration, were higher for the data subsets with lower and higher extremes of NO_y concentrations (Table 1). These conditions represent

the limiting cases of fully background conditions for the former and the strongest effects of Manaus pollution for the latter. By comparison, intermediate NO_y concentrations could arise from air masses that mixed together background air with Manaus pollution during the transport to T3 (e.g., by entrainment) and thus represent complex processing. Single or multiple mixing points could occur anywhere along the path from Manaus to T3, thus introducing variability into the effective photochemical age of the air mass arriving at T3 and resulting in lower R^2 values for intermediate NO_y concentrations. A caveat is that this explanation assumes that NO emissions from Manaus had low day-to-day variability.

In relation to the influence of Manaus pollution, sulfate concentration was affected by a mixture of background and urban sources (see discussion in Sect. 3.3) whereas NO_y concentration largely had urban sources (see Figs. 5b and 6b). As an approximation to keeping the sulfate concentration constant and thus focusing on the role of NO in the urban pollution, the visualization of the dependence of IEPOX-SOA factor loading on NO_y concentration was further refined by taking data subsets segregated by low ($< 0.1 \mu\text{g m}^{-3}$) and high ($> 0.3 \mu\text{g m}^{-3}$) sulfate concentrations. Figure 7a, b, and c show the factor loading, organic PM mass concentration, and the ratio f of the IEPOX-SOA factor loading to the organic PM mass concentration, respectively, plotted against NO_y concentration for low and high sulfate concentrations.

Figure 7a shows that for both low and high sulfate concentrations an increase in NO_y concentration from background to polluted concentrations was associated with a decrease in the IEPOX-SOA factor loading by two to three times. For low sulfate concentration, the interquartile range of the factor loading decreased from [0.037, 0.093] to [0.022, 0.039] $\mu\text{g m}^{-3}$ for an increase in NO_y concentration from 0.5 to 2 ppb. For high sulfate concentration, the factor loading decreased from [0.57, 0.95] to [0.21, 0.35] $\mu\text{g m}^{-3}$ for the same transition in NO_y concentration. The greatest changes in factor loading were in the region of 1 ppb NO_y . This region of greatest sensitivity coincided with the transition from background to polluted conditions.

For the same time period of these PM analyses of IEPOX-SOA factor loading, Liu et al. (2016a) observed a shift in dominant isoprene gas-phase products from ISOPOOH to MVK/MACR across the transition in NO_y concentration. Liu et al. (2016a) further simulated the dependence on NO concentration of the ratio of the production rate of ISOPOOH to that of MVK + MACR. The highest ratios (0.6 to 0.9) were obtained for background concentrations of NO_y . The calculated HO_2 concentration was $< 4 \times 10^8 \text{ cm}^{-3}$ (0.016 ppb). The simulated transition for the dominant fate of the ISOPOO radicals occurred for an NO concentration of < 0.05 ppb.

Figure 7b shows that for both low and high sulfate concentrations the organic PM mass concentration M_{org} and the IEPOX-SOA factor loading had opposite trends for low compared to intermediate NO_y concentrations, even though the

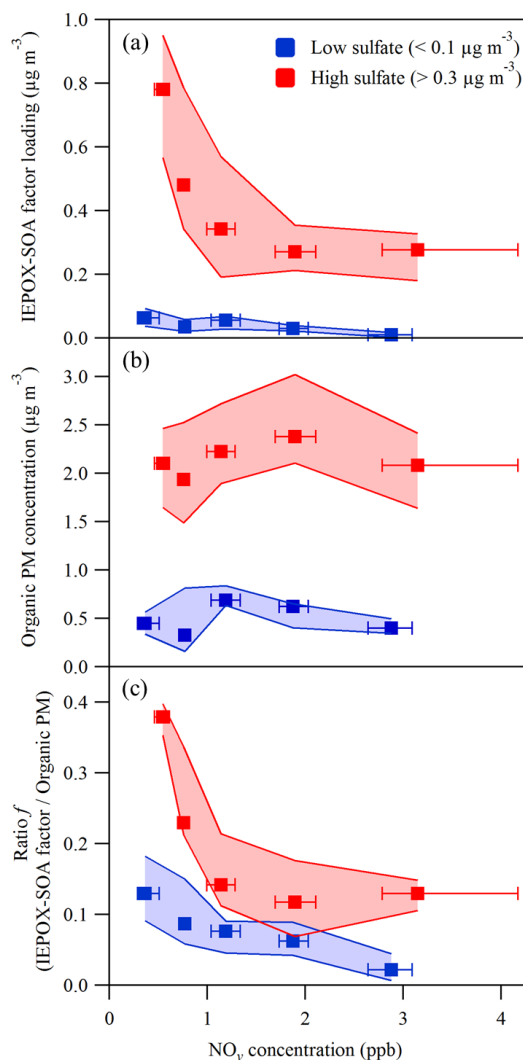


Figure 7. Dependence on NO_y concentration of (a) IEPOX-SOA factor loading, (b) organic mass concentration, and (c) the ratio f of the IEPOX-SOA factor loading to the organic PM concentration. Data are segregated by low ($< 0.1 \mu\text{g m}^{-3}$) and high ($> 0.3 \mu\text{g m}^{-3}$) sulfate mass concentration and grouped into five levels of NO_y concentration (Fig. 6). Squares represent medians of each group. Interquartile ranges are represented by whiskers along the abscissa and shading along the ordinate. The plotted data sets were recorded during local afternoon (12:00–16:00 local time; 16:00–20:00 UTC).

trend in M_{org} was less steep. The factor loadings decreased by 60 % whereas the M_{org} increased by 25 % for 0.5 to 2 ppb NO_y (Fig. 7a and b). Increases in M_{org} can include contributions from secondary PM produced by enhanced concentrations of hydroxyl radicals and ozone in the pollution plume as well as from primary PM emitted from the Manaus urban region (Martin et al., 2017; de Sá, 2017). For higher NO_y concentrations (> 2 ppb), however, Fig. 7b shows that M_{org} decreased after a peak value, approaching values close to background under the most polluted conditions. The chem-

istry can become sufficiently shifted that more-volatile gas-phase products can be produced (Pandis et al., 1991; Kroll et al., 2005; Carlton et al., 2009). In addition, hydroxyl radical concentrations can also decrease because of titration by NO₂ (Valin et al., 2013; Rohrer et al., 2014). An increase in total organic mass concentration could possibly contribute to a decrease in IEPOX-derived PM production by kinetically limiting the uptake of IEPOX (Gaston et al., 2014; Lin et al., 2014; Riva et al., 2016a). The dominant effect of the urban plume, however, seems to be that of shifting the fate of ISOPOO radicals through the increase in NO, thereby significantly decreasing the production of ISOPOOH (Liu et al., 2016a) (Sect. 3.5).

The combined trends of Fig. 7a and b for increasing NO_y are represented in Fig. 7c as the ratio f . The figure shows that f decreased for increasing NO_y concentration for both low and high sulfate concentrations. The greatest decrease occurred across the range of NO_y concentrations that represented the shift from background to polluted conditions. For low sulfate concentration, the interquartile range of f decreased from [0.09, 0.18] to [0.04, 0.09] for an increase in NO_y concentration from 0.5 to 2 ppb. These ranges shifted to [0.35, 0.40] and [0.07, 0.18] for high sulfate concentration. As a limiting statement, for the most favorable conditions with respect to the production of IEPOX-derived PM in central Amazonia (i.e., lowest NO_y and highest sulfate), f exceeded 0.40 at 25 % frequency. The implication is that at all times significant additional pathways for PM production were active. This conclusion is subject to the accuracy of the IEPOX-SOA factor loading as a scalar proxy of IEPOX-derived PM concentration (see discussion of Fig. 1 in Sect. 3.1). The magnitude of the decrease in f for high sulfate concentrations suggests that IEPOX-derived PM shifted from being a major to a minor component of the PM. Taken together, the results shown in Fig. 7 demonstrate how urban pollution affected the production and composition of regional IEPOX-derived PM.

The data sets presented in Figs. 5, 6, and 7 lead to the conclusion that the additional NO concentrations contributed by Manaus emissions typically suppress the production of IEPOX-derived PM to a greater extent than the additional sulfate concentrations enhance it. Figure 8 presents a systematic visualization. The factor loadings at T3 are represented as contours for axes of sulfate and NO_y concentrations. Higher factor loadings are favored for higher sulfate and lower NO_y concentrations. Factor loadings are most sensitive to changing concentration in the high-sulfate, low-NO_y region. The gray dashed line in Fig. 8 represents a qualitative divisor between domains of typical background and polluted conditions downwind of Manaus.

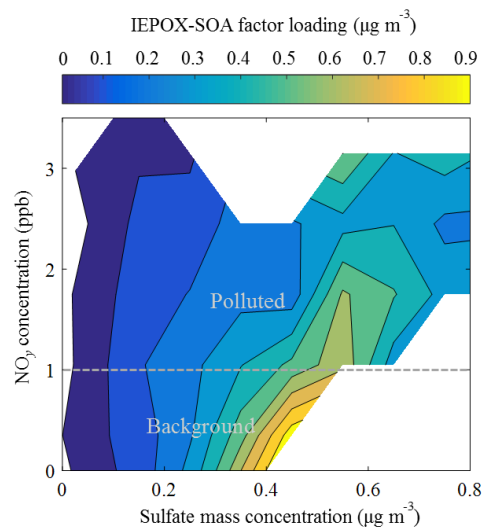


Figure 8. Contours of IEPOX-SOA factor loading for sulfate and NO_y concentrations. The plotted data were recorded during local afternoon (12:00–16:00 local time; 16:00–20:00 UTC). Typical transition between regimes of background and polluted conditions for the region downwind of Manaus are approximately represented by the dashed gray line.

3.5 Influence of NO on production and loss processes of IEPOX-derived PM

Elevated NO concentrations may affect both the production and loss processes of IEPOX-derived PM. On the one hand, production may be reduced because of increased scavenging of ISOPOO by NO, thus obviating production of IEPOX and consequently of IEPOX-derived PM. Production may also be reduced because of more rapid gas-phase loss of IEPOX in response to elevated OH and O₃ concentrations. On the other hand, loss of IEPOX-derived PM may be enhanced due to faster processing of its characteristic compounds by the elevated oxidant concentrations.

A Lagrangian model is employed to help delineate the relative importance of reduced production compared to enhanced loss on the observed IEPOX-derived PM concentrations. The model is initialized by background air that passes over Manaus in the mid-morning. The evolution of IEPOX-derived PM in that air mass is modeled under either polluted or background conditions for arrival at the T3 site in the afternoon. The governing differential equation of the model represents the sum of production and loss processes affecting the concentrations of IEPOX-derived PM, as follows:

$$\frac{dM}{dt} = -\alpha_L k_L M + \alpha_P k_P, \quad (1)$$

where M designates the IEPOX-derived PM mass concentration, t designates time, and the first and second terms on the right-hand side represent loss and production processes, respectively. Table 2 lists other symbol definitions and units.

Table 2. Descriptions and units of symbols in the model.

Symbol	Description	Unit
M	Mass concentration of IEPOX-derived PM	$\mu\text{g m}^{-3}$
t	Time	h
k_P	Zero-order rate coefficient for production under background conditions	$\mu\text{g m}^{-3} \text{h}^{-1}$
k_L	First-order rate coefficient for loss under background conditions	h^{-1}
α	Multiplicative factor representing the effects of Manaus pollution on rate coefficients	
τ	Characteristic time of a process (e.g., production, loss, or transport)	h
Subscript tr	Refers to transport	
Subscript bg	Refers to background conditions	
Subscript pol	Refers to polluted conditions	
Subscript 0	Refers to an initial state (i.e., just upwind of Manaus)	
Subscript P	Refers to production processes	
Subscript L	Refers to loss processes	

The analytic solution of Eq. (1) for time t is presented in the Supplement (Sect. S6). From this solution, characteristic times τ for production and loss processes for polluted compared to background conditions are as follows: $\tau_{P,\text{pol}} = M_0/(\alpha_P k_P)$, $\tau_{P,\text{bg}} = M_0/k_P$, $\tau_{L,\text{pol}} = 1/(\alpha_L k_L)$, and $\tau_{L,\text{bg}} = 1/k_L$ (Supplement, Sect. S6). The term M_0 represents the IEPOX-derived PM mass concentration just upwind of Manaus. Under background conditions, the enhancement factors α_L and α_P are unity by definition. Under polluted conditions, $\alpha_L = 2$ and $\alpha_P = 0.1$ to reflect enhanced loss and decreased production, respectively. Further descriptions of the model and assumptions are presented in the Supplement (Sect. S6).

The analysis strategy is to compare τ_P and τ_L to the transport time τ_{tr} under polluted and background conditions. In this way, the analysis assesses the relative importance of altered production and loss processes for IEPOX-derived PM from Manaus to T3. The statistical mode value for τ_{tr} of 4 h based on trajectory analysis is used in the model (Martin et al., 2016a). Intervals for the characteristic times τ_P and τ_L are constrained by the T3 afternoon data sets. Concentration ratios ξ , defined as $\xi = M_{\text{pol}}/M_{\text{bg}}$, are used to constrain the model (Table 3). The quantities M_{pol} and M_{bg} denote $M(t = \tau_{tr})$, meaning the mass concentration at T3 under polluted or background conditions, respectively. The use of the ratio quantity ξ in the analysis, rather than absolute concentrations, provides increased robustness because of low variability in ξ across the observed range of sulfate concentrations, even as M_{pol} and M_{bg} vary greatly (Table 3). The possible impacts of over- or underestimates of IEPOX-derived PM mass concentration, as a consequence of using IEPOX-SOA factor loading as a surrogate, are also mitigated by the use of ξ .

Two cases of the model (1 and 2) are presented, respectively focusing on constraining k_P or k_L and consequently τ_P or τ_L (Table 4). The results for Case 1 of the analysis are shown in Fig. 9a. The value of k_P is varied from 0 to $0.2 \mu\text{g m}^{-3} \text{h}^{-1}$, and the other model parameters are held con-

stant. The loss rate coefficient k_L is fixed at 0.015h^{-1} , corresponding to a characteristic time of 2.8 days (Supplement, Sect. S6). Based on observed values of ξ (gray shaded area in Fig. 9a), an interval for k_P of $[0.07, 0.13] \mu\text{g m}^{-3} \text{h}^{-1}$ is obtained, as indicated by the vertical dashed lines. Across this interval, M_{bg} and M_{pol} vary from 0.49 to $0.72 \mu\text{g m}^{-3}$ and 0.23 to $0.25 \mu\text{g m}^{-3}$, respectively, which are consistent with the observed IEPOX-SOA factor loadings (Table 3). The modeled production times have intervals of [1.8, 3.3] h for $\tau_{P,\text{bg}}$ and [18, 33] h for $\tau_{P,\text{pol}}$.

Case 2 of the analysis evaluates constraints on the loss rate coefficient k_L , and results are shown in Fig. 9b. Loss processes can include chemistry, such as heterogeneous oxidation or other in-particle reactions that reduce the IEPOX-SOA factor loading, as well as physical mechanisms, such as particle deposition and particle dilution by entrainment that reduce mass concentrations of IEPOX-derived PM (Supplement, Sect. S6). The value of k_L is varied over 3 orders of magnitude, representing characteristic times of hours to weeks, and the other model parameters are held constant (Table 4). The production rate coefficient k_P is fixed at $0.10 \mu\text{g m}^{-3} \text{h}^{-1}$, corresponding to the interval midpoint of Case 1. The observed values of ξ (gray shaded area) in intersection with the modeled values of ξ imply an upper limit on k_L at 0.043h^{-1} , corresponding to characteristic times of a day to weeks (Fig. 9b). Correspondingly, $\tau_{L,\text{bg}} > 24 \text{h}$ under background conditions, and $\tau_{L,\text{pol}} > 12 \text{h}$ under polluted conditions.

The analyses of cases 1 and 2 constrain the values of $\tau_{P,\text{pol}}$, $\tau_{P,\text{bg}}$, $\tau_{L,\text{pol}}$, and $\tau_{L,\text{bg}}$ based on the observed values of ξ . The lower limits of the characteristic times for loss, meaning $\tau_{L,\text{bg}} > 24 \text{h}$ and $\tau_{L,\text{pol}} > 12 \text{h}$, are considerably longer than the transport time of 4 h under both background and polluted conditions. Enhanced loss, therefore, does not explain alone the observed values of ξ . By comparison, the observed values of ξ imply a shift in the characteristic time for production from [1.8, 3.3] h under background conditions to [18, 33] h under pollution conditions. The shift in timescale

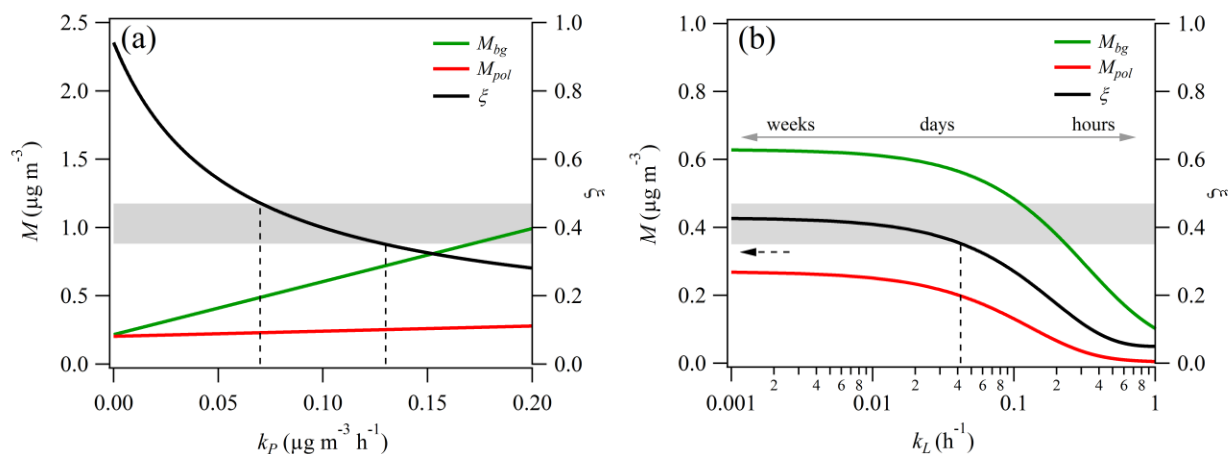


Figure 9. Modeled IEPOX-derived PM mass concentrations M_{pol} and M_{bg} at the T3 site under polluted compared to background conditions. The ratio ξ of concentrations (i.e., M_{pol}/M_{bg}) is also plotted. Panels (a, b) correspond to Case 1 and Case 2 listed in Table 4. Gray shading indicates the range of observed values of ξ across low and high sulfate concentrations. Dashed lines indicate the intersection of modeled and observed values of ξ and the corresponding constrained values of k_p or k_L along the abscissa. Labels above the double-headed arrow in (b) correspond to characteristic times (i.e., k_L^{-1}). The dashed black arrow in (b) communicates that the observed values of ξ provide no constraint on the lower limit of k_L .

Table 3. Interquartile intervals of IEPOX-SOA factor loadings observed for background and polluted conditions. Background and polluted conditions correspond to approximately 0.5 and 2 ppb of NO_y , respectively. The table also lists the resulting ratio ξ of the median factor loading under polluted compared to background conditions.

	Loading ($\mu\text{g m}^{-3}$) for background conditions		Loading ($\mu\text{g m}^{-3}$) for polluted conditions		Ratio ξ	
	Low sulfate	High sulfate	Low sulfate	High sulfate	Low sulfate	High sulfate
IEPOX-SOA factor	[0.037, 0.093]	[0.57, 0.95]	[0.022, 0.039]	[0.21, 0.35]	0.47	0.35

Table 4. Parameter values and initial conditions used for the model cases. Descriptions and units are listed in Table 2. The M_0 value is based on the mean IEPOX-SOA factor loading that was measured from 14:00 to 16:00 UTC (10:00–12:00 local time) at a regional background site during 2 months of the wet season in 2008 (Chen et al., 2015). For comparison, a similar value of $0.19 \mu\text{g m}^{-3}$ was observed during the present study as the mean at the T3 site for $\text{NO}_y < 1$ ppb (14:00–16:00 UTC).

Model case	Parameter values				Initial condition M_0
	k_p	k_L	α_p	α_L	
1. Vary k_p	0 to 0.2	0.018	0.1	3	0.23
2. Vary k_L	0.065	0.001 to 1	0.1	3	0.23

is significant in light of the transport time of 4 h. Therefore, reduced production, rather than enhanced loss, is consistent with the lower IEPOX-derived PM concentrations under polluted conditions. A few afternoon hours of altered isoprene chemistry is sufficient to significantly shift the atmospheric concentration of IEPOX-derived PM.

4 Summary and conclusions

The influence of anthropogenic emissions on the production of organic particulate matter from isoprene epoxydiols was studied during the wet season of the tropical forest in central Amazonia. The IEPOX-derived PM concentration at the T3 site, as indicated by the IEPOX-SOA factor loading, was lower under polluted compared to background conditions. Sulfate concentration was an important first-order predictor of the IEPOX-SOA factor loading, corroborating the understanding of the role of sulfate in the production of IEPOX-derived PM that has been developed in laboratory studies as well as in investigations in the southeastern USA (Surratt et al., 2007b; Budisulistiorini et al., 2013, 2015; Hu et al., 2015; Kuwata et al., 2015; Xu et al., 2015). Unlike the southeastern USA, however, where anthropogenic influences dominated variability in sulfate concentrations, contributions by the Manaus urban region to sulfate concentrations were of approximately equal magnitude to the background variability in central Amazonia. By comparison, Manaus urban emissions of NO dominated over background concentrations, and

the NO_y concentration measured 4 to 6 h downwind of Manaus at the T3 site was an important predictor of the IEPOX-SOA factor loading. In net effect, the suppression of IEPOX production because of elevated NO concentrations in the pollution plume dominated over any enhancements in IEPOX uptake because of greater sulfate concentrations.

The dependence of the IEPOX-SOA factor loadings on both sulfate and NO_y concentrations, as shown in Fig. 8, suggests that altered net anthropogenic effects may be expected for different geographic regions, even within Amazonia, and different time periods, such as the wet and dry seasons. The T3 site experienced a wide range of NO_y concentrations, allowing for the systematic demonstration of the dependence of IEPOX-derived PM concentrations on NO_y concentrations. The results show that the transition in isoprene photochemistry related to the production of IEPOX-derived PM is most sensitive precisely at the transition between background and polluted conditions, around 1 ppb of NO_y , at least for central Amazonia in the wet season. These findings suggest that the fraction of PM derived from IEPOX might be lower and have lower variability for other geographic regions characterized by higher NO_y baseline concentrations (e.g., upward of 1 to 2 ppb). For regions further downwind of the urban center, the effects of the plume are expected to phase out both due to dilution and to consumption of NO, and a gradual transition to background chemistry is expected to take place. Adequately representing background conditions and the transition to polluted conditions within models, including the dependence of the production of IEPOX-derived PM not only on sulfate but also on NO concentration, is thus important for making accurate predictions of PM concentrations, both in Amazonia and around the globe.

The findings herein can be considered in the context of Amazonia in transition (Davidson et al., 2012). In the past 50 years, the metropolitan area of Manaus, today at more than 2 million inhabitants, has experienced rapid economic and population growth (Martin et al., 2016a). Changes in the fuel matrix, such as the ongoing shift from high-sulfur to low-sulfur oil in the vehicle fleet as well as from fuel oil to natural gas in many power plants (Medeiros et al., 2017), are changing the composition of the Manaus pollution plume. Based on the findings presented herein, a reduction in sulfate sources from Manaus, whether primary or secondary, would not be expected to considerably affect the mass concentration of IEPOX-derived species in forest regions affected by the plume. Background sources independent of Manaus appear sufficient to sustain sulfate concentrations regionally. In the absence of pollution-control technologies, however, NO emissions can be expected to increase in coming years due to the development of more efficient (i.e., higher temperature) sources of electricity associated with the development of natural gas resources in the basin, as well as from growth in transportation associated with increased population. Increased NO concentrations can be expected to reduce the mass concentration of IEPOX-derived species in forest

regions affected by the plume. Changes in the atmospheric particle population can have follow-up effects on cloud type, duration, and rainfall (Pöschl et al., 2010). In addition to PM derived from IEPOX as discussed herein, a better understanding of other pathways that also contribute to organic PM, as well as possible changes to those pathways with increasing pollution in the region, warrants further study so as to achieve sufficient knowledge for decision-making related to air quality and climate in Amazonia.

Data availability. The data sets used in this publication are available at the ARM Climate Research Facility database for the GoAmazon2014/5 experiment (<https://www.arm.gov/research/campaigns/amf2014goamazon>).

The Supplement related to this article is available online at <https://doi.org/10.5194/acp-17-6611-2017-supplement>.

Competing interests. The authors declare that they have no conflict of interest.

Acknowledgements. Institutional support was provided by the Central Office of the Large Scale Biosphere Atmosphere Experiment in Amazonia (LBA), the National Institute of Amazonian Research (INPA), and Amazonas State University (UEA). We acknowledge support from the Atmospheric Radiation Measurement (ARM) Climate Research Facility, a user facility of the United States Department of Energy (DOE), Office of Science, sponsored by the Office of Biological and Environmental Research, and support from the Atmospheric System Research (ASR) program of that office. Additional funding was provided by the Amazonas State Research Foundation (FAPEAM), the São Paulo State Research Foundation (FAPESP), the USA National Science Foundation (NSF), and the Brazilian Scientific Mobility Program (CsF/CAPES). S. de Sá acknowledges support by the Schlumberger Foundation, Faculty for the Future Fellowship. The research was conducted under scientific license 001030/2012-4 of the Brazilian National Council for Scientific and Technological Development (CNPq).

Edited by: T. Karl

Reviewed by: two anonymous referees

References

- Andreae, M., Berresheim, H., Bingemer, H., Jacob, D. J., Lewis, B., Li, S. M., and Talbot, R. W.: The atmospheric sulfur cycle over the Amazon Basin: 2. Wet season, *J. Geophys. Res.-Atmos.*, 95, 16813–16824, <https://doi.org/10.1029/JD095iD10p16813>, 1990.
- Andreae, M. O., Acevedo, O. C., Araújo, A., Artaxo, P., Barbosa, C. G. G., Barbosa, H. M. J., Brito, J., Carbone, S., Chi, X., Cintra, B. B. L., da Silva, N. F., Dias, N. L., Dias-Júnior, C. Q., Ditas, F., Ditz, R., Godoi, A. F. L., Godoi, R. H. M., Heimann, M., Hoffmann, T., Kesselmeier, J., Könnemann, T., Krüger, M. L., Lavric,

- J. V., Manzi, A. O., Lopes, A. P., Martins, D. L., Mikhailov, E. F., Moran-Zuloaga, D., Nelson, B. W., Nölscher, A. C., Santos Nogueira, D., Piedade, M. T. F., Pöhlker, C., Pöschl, U., Quesada, C. A., Rizzo, L. V., Ro, C.-U., Ruckteschler, N., Sá, L. D. A., de Oliveira Sá, M., Sales, C. B., dos Santos, R. M. N., Saturno, J., Schöngart, J., Sörgel, M., de Souza, C. M., de Souza, R. A. F., Su, H., Targhetta, N., Töta, J., Trebs, I., Trumbore, S., van Eijck, A., Walter, D., Wang, Z., Weber, B., Williams, J., Winderlich, J., Wittmann, F., Wolff, S., and Yáñez-Serrano, A. M.: The Amazon Tall Tower Observatory (ATTO): overview of pilot measurements on ecosystem ecology, meteorology, trace gases, and aerosols, *Atmos. Chem. Phys.*, 15, 10723–10776, <https://doi.org/10.5194/acp-15-10723-2015>, 2015.
- Bakwin, P. S., Wofsy, S. C., Fan, S. M., Keller, M., Trumbore, S. E., and Da Costa, J. M.: Emission of nitric oxide (NO) from tropical forest soils and exchange of NO between the forest canopy and atmospheric boundary layers, *J. Geophys. Res.-Atmos.*, 95, 16755–16764, <https://doi.org/10.1029/JD095iD10p16755>, 1990.
- Bateman, A. P., Gong, Z., Liu, P., Sato, B., Cirino, G., Zhang, Y., Artaxo, P., Bertram, A. K., Manzi, A. O., Rizzo, L. V., Souza, R. A. F., Zaveri, R. A., and Martin, S. T.: Sub-micrometre particulate matter is primarily in liquid form over Amazon rainforest, *Nat. Geosci.*, 9, 34–37, <https://doi.org/10.1038/ngeo2599>, 2016.
- Budisulistiorini, S. H., Canagaratna, M. R., Croteau, P. L., Marth, W. J., Baumann, K., Edgerton, E. S., Shaw, S. L., Knipping, E. M., Worsnop, D. R., Jayne, J. T., Gold, A., and Surratt, J. D.: Real-time continuous characterization of secondary organic aerosol derived from isoprene epoxydiols in downtown Atlanta, Georgia, using the Aerodyne Aerosol Chemical Speciation Monitor, *Environ. Sci. Technol.*, 47, 5686–5694, <https://doi.org/10.1021/es400023n>, 2013.
- Budisulistiorini, S. H., Li, X., Bairai, S. T., Renfro, J., Liu, Y., Liu, Y. J., McKinney, K. A., Martin, S. T., McNeill, V. F., Pye, H. O. T., Nenes, A., Neff, M. E., Stone, E. A., Mueller, S., Knote, C., Shaw, S. L., Zhang, Z., Gold, A., and Surratt, J. D.: Examining the effects of anthropogenic emissions on isoprene-derived secondary organic aerosol formation during the 2013 Southern Oxidant and Aerosol Study (SOAS) at the Look Rock, Tennessee ground site, *Atmos. Chem. Phys.*, 15, 8871–8888, <https://doi.org/10.5194/acp-15-8871-2015>, 2015.
- Budisulistiorini, S. H., Baumann, K., Edgerton, E. S., Bairai, S. T., Mueller, S., Shaw, S. L., Knipping, E. M., Gold, A., and Surratt, J. D.: Seasonal characterization of submicron aerosol chemical composition and organic aerosol sources in the southeastern United States: Atlanta, Georgia, and Look Rock, Tennessee, *Atmos. Chem. Phys.*, 16, 5171–5189, <https://doi.org/10.5194/acp-16-5171-2016>, 2016.
- Canagaratna, M. R., Jayne, J. T., Jimenez, J. L., Allan, J. D., Alfarra, M. R., Zhang, Q., Onasch, T. B., Drewnick, F., Coe, H., Middlebrook, A., Delia, A., Williams, L. R., Trimborn, A. M., Northway, M. J., DeCarlo, P. F., Kolb, C. E., Davidovits, P., and Worsnop, D. R.: Chemical and microphysical characterization of ambient aerosols with the aerodyne aerosol mass spectrometer, *Mass Spectrom. Rev.*, 26, 185–222, <https://doi.org/10.1002/mas.20115>, 2007.
- Carbone, S., Brito, J. F., Xu, L., Ng, N. L., Rizzo, L., Cirino, G., Holanda, B., Wolff, S., Saturno, J., Chi, X., Souza, R. A. F., Arana, A., de Sá, M., Krüger, M., Andreae, M. O., Pöhlker, C., Barbosa, H. M. J., and Artaxo, P.: Long-term chemical composition and source apportionment of submicron aerosol particles in the central Amazon basin (ATTO), in preparation, 2017.
- Carlton, A. G., Wiedinmyer, C., and Kroll, J. H.: A review of Secondary Organic Aerosol (SOA) formation from isoprene, *Atmos. Chem. Phys.*, 9, 4987–5005, <https://doi.org/10.5194/acp-9-4987-2009>, 2009.
- Chen, Q., Farmer, D. K., Schneider, J., Zorn, S. R., Heald, C. L., Karl, T. G., Guenther, A., Allan, J. D., Robinson, N., Coe, H., Kimmel, J. R., Pauliquevis, T., Borrmann, S., Pöschl, U., Andreae, M. O., Artaxo, P., Jimenez, J. L., and Martin, S. T.: Mass spectral characterization of submicron biogenic organic particles in the Amazon Basin, *Geophys. Res. Lett.*, 36, L20806, <https://doi.org/10.1029/2009GL039880>, 2009.
- Chen, Q., Farmer, D. K., Rizzo, L. V., Pauliquevis, T., Kuwata, M., Karl, T. G., Guenther, A., Allan, J. D., Coe, H., Andreae, M. O., Pöschl, U., Jimenez, J. L., Artaxo, P., and Martin, S. T.: Submicron particle mass concentrations and sources in the Amazonian wet season (AMAZE-08), *Atmos. Chem. Phys.*, 15, 3687–3701, <https://doi.org/10.5194/acp-15-3687-2015>, 2015.
- Claeys, M., Graham, B., Vas, G., Wang, W., Vermeylen, R., Pashynska, V., Cafmeyer, J., Guyon, P., Andreae, M. O., Artaxo, P., and Maenhaut, W.: Formation of secondary organic aerosols through photooxidation of isoprene, *Science*, 303, 1173–1176, <https://doi.org/10.1126/science.1092805>, 2004.
- Crouse, J. D., Paulot, F., Kjaergaard, H. G., and Wennberg, P. O.: Peroxy radical isomerization in the oxidation of isoprene, *Phys. Chem. Chem. Phys.*, 13, 13607–13613, <https://doi.org/10.1039/C1CP21330J>, 2011.
- Davidson, E. A., de Araújo, A. C., Artaxo, P., Balch, J. K., Brown, I. F., Bustamante, M. M., Coe, M. T., DeFries, R. S., Keller, M., and Longo, M.: The Amazon basin in transition, *Nature*, 481, 321–328, 2012.
- DeCarlo, P. F., Kimmel, J. R., Trimborn, A., Northway, M. J., Jayne, J. T., Aiken, A. C., Gonin, M., Fuhrer, K., Horvath, T., Docherty, K. S., Worsnop, D. R., and Jimenez, J. L.: Field-deployable, high-resolution, time-of-flight aerosol mass spectrometer, *Anal. Chem.*, 78, 8281–8289, <https://doi.org/10.1021/ac061249n>, 2006.
- de Sá, S. S.: Anthropogenic emissions affect the sources and composition of submicron particulate matter in central Amazonia in the wet season, in preparation, 2017.
- Ervens, B. and Volkamer, R.: Glyoxal processing by aerosol multiphase chemistry: towards a kinetic modeling framework of secondary organic aerosol formation in aqueous particles, *Atmos. Chem. Phys.*, 10, 8219–8244, <https://doi.org/10.5194/acp-10-8219-2010>, 2010.
- Ervens, B., Turpin, B. J., and Weber, R. J.: Secondary organic aerosol formation in cloud droplets and aqueous particles (aq-SOA): a review of laboratory, field and model studies, *Atmos. Chem. Phys.*, 11, 11069–11102, <https://doi.org/10.5194/acp-11-11069-2011>, 2011.
- Fu, T. M., Jacob, D. J., Wittrock, F., Burrows, J. P., Vrekoussis, M., and Henze, D. K.: Global budgets of atmospheric glyoxal and methylglyoxal, and implications for formation of secondary organic aerosols, *J. Geophys. Res.-Atmos.*, 113, D15303, <https://doi.org/10.1029/2007JD009505>, 2008.
- Gaston, C. J., Riedel, T. P., Zhang, Z., Gold, A., Surratt, J. D., and Thornton, J. A.: Reactive uptake of an isoprene-derived epoxy-

- diol to submicron aerosol particles, *Environ. Sci. Technol.*, 48, 11178–11186, <https://doi.org/10.1021/es5034266>, 2014.
- Guenther, A. B., Jiang, X., Heald, C. L., Sakulyanontvittaya, T., Duhl, T., Emmons, L. K., and Wang, X.: The Model of Emissions of Gases and Aerosols from Nature version 2.1 (MEGAN2.1): an extended and updated framework for modeling biogenic emissions, *Geosci. Model Dev.*, 5, 1471–1492, <https://doi.org/10.5194/gmd-5-1471-2012>, 2012.
- Hallquist, M., Wenger, J. C., Baltensperger, U., Rudich, Y., Simpson, D., Claeys, M., Dommen, J., Donahue, N. M., George, C., Goldstein, A. H., Hamilton, J. F., Herrmann, H., Hoffmann, T., Iinuma, Y., Jang, M., Jenkin, M. E., Jimenez, J. L., Kiendler-Scharr, A., Maenhaut, W., McFiggans, G., Mentel, Th. F., Monod, A., Prévôt, A. S. H., Seinfeld, J. H., Surratt, J. D., Szmigielski, R., and Wildt, J.: The formation, properties and impact of secondary organic aerosol: current and emerging issues, *Atmos. Chem. Phys.*, 9, 5155–5236, <https://doi.org/10.5194/acp-9-5155-2009>, 2009.
- Hu, W. W., Campuzano-Jost, P., Palm, B. B., Day, D. A., Ortega, A. M., Hayes, P. L., Krechmer, J. E., Chen, Q., Kuwata, M., Liu, Y. J., de Sá, S. S., McKinney, K., Martin, S. T., Hu, M., Budisulistiorini, S. H., Riva, M., Surratt, J. D., St. Clair, J. M., Isaacman-Van Wertz, G., Yee, L. D., Goldstein, A. H., Carbone, S., Brito, J., Artaxo, P., de Gouw, J. A., Koss, A., Wisthaler, A., Mikoviny, T., Karl, T., Kaser, L., Jud, W., Hansel, A., Docherty, K. S., Alexander, M. L., Robinson, N. H., Coe, H., Allan, J. D., Canagaratna, M. R., Paulot, F., and Jimenez, J. L.: Characterization of a real-time tracer for isoprene epoxydiols-derived secondary organic aerosol (IEPOX-SOA) from aerosol mass spectrometer measurements, *Atmos. Chem. Phys.*, 15, 11807–11833, <https://doi.org/10.5194/acp-15-11807-2015>, 2015.
- Hu, W., Palm, B. B., Day, D. A., Campuzano-Jost, P., Krechmer, J. E., Peng, Z., de Sá, S. S., Martin, S. T., Alexander, M. L., Baumann, K., Hacker, L., Kiendler-Scharr, A., Koss, A. R., de Gouw, J. A., Goldstein, A. H., Seco, R., Sjostedt, S. J., Park, J.-H., Guenther, A. B., Kim, S., Canonaco, F., Prévôt, A. S. H., Brune, W. H., and Jimenez, J. L.: Volatility and lifetime against OH heterogeneous reaction of ambient isoprene-epoxydiols-derived secondary organic aerosol (IEPOX-SOA), *Atmos. Chem. Phys.*, 16, 11563–11580, <https://doi.org/10.5194/acp-16-11563-2016>, 2016.
- Isaacman, G., Kreisberg, N. M., Yee, L. D., Worton, D. R., Chan, A. W. H., Moss, J. A., Hering, S. V., and Goldstein, A. H.: On-line derivatization for hourly measurements of gas- and particle-phase semi-volatile oxygenated organic compounds by thermal desorption aerosol gas chromatography (SV-TAG), *Atmos. Meas. Tech.*, 7, 4417–4429, <https://doi.org/10.5194/amt-7-4417-2014>, 2014.
- Isaacman-VanWertz, G., Yee, L. D., Kreisberg, N. M., Wernis, R., Moss, J. A., Hering, S. V., de Sá, S. S., Martin, S. T., Alexander, M. L., Palm, B. B., Hu, W., Campuzano-Jost, P., Day, D. A., Jimenez, J. L., Riva, M., Surratt, J. D., Viegas, J., Manzi, A., Edgerton, E., Baumann, K., Souza, R., Artaxo, P., and Goldstein, A. H.: Ambient Gas-Particle Partitioning of Tracers for Biogenic Oxidation, *Environ. Sci. Technol.*, 50, 9952–9962, <https://doi.org/10.1021/acs.est.6b01674>, 2016.
- Jacob, D. J. and Wofsy, S. C.: Budgets of reactive nitrogen, hydrocarbons, and ozone over the Amazon forest during the wet season, *J. Geophys. Res.-Atmos.*, 95, 16737–16754, <https://doi.org/10.1029/JD095iD10p16737>, 1990.
- Jacobs, M. I., Burke, W. J., and Elrod, M. J.: Kinetics of the reactions of isoprene-derived hydroxynitrates: gas phase epoxide formation and solution phase hydrolysis, *Atmos. Chem. Phys.*, 14, 8933–8946, <https://doi.org/10.5194/acp-14-8933-2014>, 2014.
- Jimenez, J. L., Canagaratna, M. R., Donahue, N. M., Prevot, A. S. H., Zhang, Q., Kroll, J. H., DeCarlo, P. F., Allan, J. D., Coe, H., Ng, N. L., Aiken, A. C., Docherty, K. S., Ulbrich, I. M., Grieshop, A. P., Robinson, A. L., Duplissy, J., Smith, J. D., Wilson, K. R., Lanz, V. A., Hueglin, C., Sun, Y. L., Tian, J., Laaksonen, A., Raatikainen, T., Rautiainen, J., Vaattovaara, P., Ehn, M., Kulmala, M., Tomlinson, J. M., Collins, D. R., Cubison, M. J., Dunlea, J., Huffman, J. A., Onasch, T. B., Alfarra, M. R., Williams, P. I., Bower, K., Kondo, Y., Schneider, J., Drewnick, F., Borrmann, S., Weimer, S., Demerjian, K., Salcedo, D., Cottrell, L., Griffin, R., Takami, A., Miyoshi, T., Hatakeyama, S., Shimono, A., Sun, J. Y., Zhang, Y. M., Dzepina, K., Kimmel, J. R., Sueper, D., Jayne, J. T., Herndon, S. C., Trimborn, A. M., Williams, L. R., Wood, E. C., Middlebrook, A. M., Kolb, C. E., Baltensperger, U., and Worsnop, D. R.: Evolution of organic aerosols in the atmosphere, *Science*, 326, 1525–1529, <https://doi.org/10.1126/science.1180353>, 2009.
- Kanakidou, M., Seinfeld, J. H., Pandis, S. N., Barnes, I., Dentener, F. J., Facchini, M. C., Van Dingenen, R., Ervens, B., Nenes, A., Nielsen, C. J., Swietlicki, E., Putaud, J. P., Balkanski, Y., Fuzzi, S., Horth, J., Moortgat, G. K., Winterhalter, R., Myhre, C. E. L., Tsigaridis, K., Vignati, E., Stephanou, E. G., and Wilson, J.: Organic aerosol and global climate modelling: a review, *Atmos. Chem. Phys.*, 5, 1053–1123, <https://doi.org/10.5194/acp-5-1053-2005>, 2005.
- Kaufman, Y. J., Tanré, D., and Boucher, O.: A satellite view of aerosols in the climate system, *Nature*, 419, 215–223, 2002.
- Kjaergaard, H. G., Knap, H. C., Ørnso, K. B., Jørgensen, S., Crounse, J. D., Paulot, F., and Wennberg, P. O.: Atmospheric Fate of Methacrolein. 2. Formation of Lactone and Implications for Organic Aerosol Production, *J. Phys. Chem. A*, 116, 5763–5768, <https://doi.org/10.1021/jp210853h>, 2012.
- Krechmer, J. E., Coggon, M. M., Massoli, P., Nguyen, T. B., Crounse, J. D., Hu, W., Day, D. A., Tyndall, G. S., Henze, D. K., Rivera-Rios, J. C., Nowak, J. B., Kimmel, J. R., Mauldin, R. L., Stark, H., Jayne, J. T., Sipilä, M., Junninen, H., Clair, J. M. S., Zhang, X., Feiner, P. A., Zhang, L., Miller, D. O., Brune, W. H., Keutsch, F. N., Wennberg, P. O., Seinfeld, J. H., Worsnop, D. R., Jimenez, J. L., and Canagaratna, M. R.: Formation of low volatility organic compounds and secondary organic aerosol from isoprene hydroxyhydroperoxide low-NO oxidation, *Environ. Sci. Technol.*, 49, 10330–10339, <https://doi.org/10.1021/acs.est.5b02031>, 2015.
- Kroll, J. H., Ng, N. L., Murphy, S. M., Flagan, R. C., and Seinfeld, J. H.: Secondary organic aerosol formation from isoprene photooxidation under high-NO_x conditions, *Geophys. Res. Lett.*, 32, L18808, <https://doi.org/10.1029/2005GL023637>, 2005.
- Kuhn, U., Ganzeveld, L., Thielmann, A., Dindorf, T., Schebeske, G., Welling, M., Sciare, J., Roberts, G., Meixner, F. X., Kesselmeier, J., Lelieveld, J., Kolle, O., Ciccioli, P., Lloyd, J., Trentmann, J., Artaxo, P., and Andreae, M. O.: Impact of Manaus City on the Amazon Green Ocean atmosphere: ozone production,

- precursor sensitivity and aerosol load, *Atmos. Chem. Phys.*, 10, 9251–9282, <https://doi.org/10.5194/acp-10-9251-2010>, 2010.
- Kuwata, M., Liu, Y., McKinney, K., and Martin, S. T.: Physical state and acidity of inorganic sulfate can regulate the production of secondary organic material from isoprene photooxidation products, *Phys. Chem. Chem. Phys.*, 17, 5670–5678, <https://doi.org/10.1039/C4CP04942J>, 2015.
- Levine, J. G., MacKenzie, A. R., Squire, O. J., Archibald, A. T., Griffiths, P. T., Abraham, N. L., Pyle, J. A., Oram, D. E., Forster, G., Brito, J. F., Lee, J. D., Hopkins, J. R., Lewis, A. C., Bauguitte, S. J. B., Demarco, C. F., Artaxo, P., Messina, P., Lathière, J., Hauglustaine, D. A., House, E., Hewitt, C. N., and Nemitz, E.: Isoprene chemistry in pristine and polluted Amazon environments: Eulerian and Lagrangian model frameworks and the strong bearing they have on our understanding of surface ozone and predictions of rainforest exposure to this priority pollutant, *Atmos. Chem. Phys. Discuss.*, 15, 24251–24310, <https://doi.org/10.5194/acpd-15-24251-2015>, 2015.
- Lewandowski, M., Jaoui, M., Offenberg, J. H., Krug, J. D., and Kleindienst, T. E.: Atmospheric oxidation of isoprene and 1,3-butadiene: influence of aerosol acidity and relative humidity on secondary organic aerosol, *Atmos. Chem. Phys.*, 15, 3773–3783, <https://doi.org/10.5194/acp-15-3773-2015>, 2015.
- Lim, H.-J., Carlton, A. G., and Turpin, B. J.: Isoprene forms secondary organic aerosol through cloud processing: Model simulations, *Environ. Sci. Technol.*, 39, 4441–4446, <https://doi.org/10.1021/es048039h>, 2005.
- Lin, Y.-H., Zhang, Z., Docherty, K. S., Zhang, H., Budisulistiorini, S. H., Rubitschun, C. L., Shaw, S. L., Knipping, E. M., Edgerton, E. S., Kleindienst, T. E., Gold, A., and Surratt, J. D.: Isoprene epoxydiols as precursors to secondary organic aerosol formation: acid-catalyzed reactive uptake studies with authentic compounds, *Environ. Sci. Technol.*, 46, 250–258, <https://doi.org/10.1021/es202554c>, 2012.
- Lin, Y.-H., Zhang, H., Pye, H. O. T., Zhang, Z., Marth, W. J., Park, S., Arashiro, M., Cui, T., Budisulistiorini, S. H., Sexton, K. G., Vizuete, W., Xie, Y., Luecken, D. J., Piletic, I. R., Edney, E. O., Bartolotti, L. J., Gold, A., and Surratt, J. D.: Epoxide as a precursor to secondary organic aerosol formation from isoprene photooxidation in the presence of nitrogen oxides, *P. Natl. Acad. Sci. USA*, 110, 6718–6723, <https://doi.org/10.1073/pnas.1221150110>, 2013.
- Lin, Y.-H., Budisulistiorini, S. H., Chu, K., Siejack, R. A., Zhang, H., Riva, M., Zhang, Z., Gold, A., Kautzman, K. E., and Surratt, J. D.: Light-absorbing oligomer formation in secondary organic aerosol from reactive uptake of isoprene epoxydiols, *Environ. Sci. Technol.*, 48, 12012–12021, <https://doi.org/10.1021/es503142b>, 2014.
- Liu, Y., Kuwata, M., Strick, B. F., Geiger, F. M., Thomson, R. J., McKinney, K. A., and Martin, S. T.: Uptake of epoxydiol isomers accounts for half of the particle-phase material produced from isoprene photooxidation via the HO₂ pathway, *Environ. Sci. Technol.*, 49, 250–258, <https://doi.org/10.1021/es5034298>, 2015.
- Liu, Y., Brito, J., Dorris, M. R., Rivera-Rios, J. C., Seco, R., Bates, K. H., Artaxo, P., Duvoisin, S., Keutsch, F. N., Kim, S., Goldstein, A. H., Guenther, A. B., Manzi, A. O., Souza, R. A. F., Springston, S. R., Watson, T. B., McKinney, K. A., and Martin, S. T.: Isoprene photochemistry over the Amazon rain forest, *P. Natl. Acad. Sci. USA*, 113, 6125–6130, <https://doi.org/10.1073/pnas.1524136113>, 2016a.
- Liu, J., D'Ambro, E. L., Lee, B. H., Lopez-Hilfiker, F. D., Zaveri, R. A., Rivera-Rios, J. C., Keutsch, F. N., Iyer, S., Kurten, T., Zhang, Z., Gold, A., Surratt, J. D., Shilling, J. E., and Thornton, J. A.: Efficient Isoprene Secondary Organic Aerosol Formation from a Non-IEPOX Pathway, *Environ. Sci. Technol.*, 50, 9872–9880, <https://doi.org/10.1021/acs.est.6b01872>, 2016b.
- Liu, Y., Kuwata, M., McKinney, K. A., and Martin, S. T.: Uptake and release of gaseous species accompanying the reactions of isoprene photo-oxidation products with sulfate particles, *Phys. Chem. Chem. Phys.*, 18, 1595–1600, <https://doi.org/10.1039/C5CP04551G>, 2016c.
- Liu, Y. J., Herdinger-Blatt, I., McKinney, K. A., and Martin, S. T.: Production of methyl vinyl ketone and methacrolein via the hydroperoxyl pathway of isoprene oxidation, *Atmos. Chem. Phys.*, 13, 5715–5730, <https://doi.org/10.5194/acp-13-5715-2013>, 2013.
- Lopez-Hilfiker, F. D., Mohr, C., D'Ambro, E. L., Lutz, A., Riedel, T. P., Gaston, C. J., Iyer, S., Zhang, Z., Gold, A., Surratt, J. D., Lee, B. H., Kurten, T., Hu, W. W., Jimenez, J., Hallquist, M., and Thornton, J. A.: Molecular composition and volatility of organic aerosol in the Southeastern US: implications for IEPOX derived SOA, *Environ. Sci. Technol.*, 50, 2200–2209, <https://doi.org/10.1021/acs.est.5b04769>, 2016.
- Marais, E. A., Jacob, D. J., Jimenez, J. L., Campuzano-Jost, P., Day, D. A., Hu, W., Krechmer, J., Zhu, L., Kim, P. S., Miller, C. C., Fisher, J. A., Travis, K., Yu, K., Hanisco, T. F., Wolfe, G. M., Arkinson, H. L., Pye, H. O. T., Froyd, K. D., Liao, J., and McNeill, V. F.: Aqueous-phase mechanism for secondary organic aerosol formation from isoprene: application to the southeast United States and co-benefit of SO₂ emission controls, *Atmos. Chem. Phys.*, 16, 1603–1618, <https://doi.org/10.5194/acp-16-1603-2016>, 2016.
- Martin, S. T., Andreae, M. O., Artaxo, P., Baumgardner, D., Chen, Q., Goldstein, A. H., Guenther, A., Heald, C. L., Mayol-Bracero, O. L., McMurry, P. H., Pauliquevis, T., Pöschl, U., Prather, K. A., Roberts, G. C., Saleska, S. R., Silva Dias, M. A., Spracklen, D. V., Swietlicki, E., and Trebs, I.: Sources and properties of Amazonian aerosol particles, *Rev. Geophys.*, 48, RG2012, <https://doi.org/10.1029/2008RG000280>, 2010a.
- Martin, S. T., Andreae, M. O., Althausen, D., Artaxo, P., Baars, H., Borrmann, S., Chen, Q., Farmer, D. K., Guenther, A., Gunthe, S. S., Jimenez, J. L., Karl, T., Longo, K., Manzi, A., Müller, T., Pauliquevis, T., Petters, M. D., Prenni, A. J., Pöschl, U., Rizzo, L. V., Schneider, J., Smith, J. N., Swietlicki, E., Tota, J., Wang, J., Wiedensohler, A., and Zorn, S. R.: An overview of the Amazonian Aerosol Characterization Experiment 2008 (AMAZE-08), *Atmos. Chem. Phys.*, 10, 11415–11438, <https://doi.org/10.5194/acp-10-11415-2010>, 2010b.
- Martin, S. T., Artaxo, P., Machado, L. A. T., Manzi, A. O., Souza, R. A. F., Schumacher, C., Wang, J., Andreae, M. O., Barbosa, H. M. J., Fan, J., Fisch, G., Goldstein, A. H., Guenther, A., Jimenez, J. L., Pöschl, U., Silva Dias, M. A., Smith, J. N., and Wendisch, M.: Introduction: Observations and Modeling of the Green Ocean Amazon (GoAmazon2014/5), *Atmos. Chem. Phys.*, 16, 4785–4797, <https://doi.org/10.5194/acp-16-4785-2016>, 2016a.
- Martin, S. T., Artaxo, P. E., Chen, Q., Guenther, A. B., Gunthe, S. S., Jimenez, J. L., Manzi, A., Prenni, K. L., Pöschl, U., Schnei-

- der, J., and Swietlicki, E.: AMAZE-08 Aerosol Characterization and Meteorological Data, Central Amazon Basin: 2008, ORNL Distributed Active Archive Center, 2016b.
- Martin, S. T., Artaxo, P., Machado, L., Manzi, A. O., Souza, R. A. F., Schumacher, C., Wang, J., Biscaro, T., Brito, J., Calheiros, A., Jardine, K., Medeiros, A., Portela, B., Sá, S. S. d., Adachi, K., Aiken, A. C., Albrecht, R., Alexander, L., Andreae, M. O., Barbosa, H. M. J., Buseck, P., Chand, D., Comstock, J. M., Day, D. A., Dubey, M., Fan, J., Fast, J., Fisch, G., Fortner, E., Giangrande, S., Gilles, M., Goldstein, A. H., Guenther, A., Hubbe, J., Jensen, M., Jimenez, J. L., Keutsch, F. N., Kim, S., Kuang, C., Laskin, A., McKinney, K., Mei, F., Miller, M., Nascimento, R., Pauliquevis, T., Pekour, M., Peres, J., Petäjä, T., Pöhlker, C., Pöschl, U., Rizzo, L., Schmid, B., Shilling, J. E., Dias, M. A. S., Smith, J. N., Tomlinson, J. M., Tóta, J., and Wendisch, M.: The Green ocean Amazon Experiment (GoAmazon2014/5) observes pollution affecting gases, aerosols, clouds, and rainfall over the rain forest, *B. Am. Meteorol. Soc.*, 98, 981–997, <https://doi.org/10.1175/BAMS-D-15-00221.1>, 2017.
- Mather, J. H. and Voyles, J. W.: The ARM Climate Research Facility: A review of structure and capabilities, *B. Am. Meteorol. Soc.*, 94, 377–392, <https://doi.org/10.1175/BAMS-D-11-00218.1>, 2013.
- McNeill, V. F., Woo, J. L., Kim, D. D., Schwier, A. N., Wannell, N. J., Sumner, A. J., and Barakat, J. M.: Aqueous-phase secondary organic aerosol and organosulfate formation in atmospheric aerosols: a modeling study, *Environ. Sci. Technol.*, 46, 8075–8081, <https://doi.org/10.1021/es3002986>, 2012.
- Medeiros, A. S. S., Calderaro, G., Guimarães, P. C., Magalhaes, M. R., Morais, M. V. B., Rafee, S. A. A., Ribeiro, I. O., Andreoli, R. V., Martins, J. A., Martins, L. D., Martin, S. T., and Souza, R. A. F.: Power Plant Fuel Switching and Air Quality in a Tropical Forested Environment, *Atmos. Chem. Phys. Discuss.*, <https://doi.org/10.5194/acp-2016-1113>, in review, 2017.
- Nel, A.: Air pollution-related illness: effects of particles, *Science*, 308, 804–806, 2005.
- Nguyen, T. B., Coggon, M. M., Bates, K. H., Zhang, X., Schwantes, R. H., Schilling, K. A., Loza, C. L., Flagan, R. C., Wennberg, P. O., and Seinfeld, J. H.: Organic aerosol formation from the reactive uptake of isoprene epoxydiols (IEPOX) onto non-acidified inorganic seeds, *Atmos. Chem. Phys.*, 14, 3497–3510, <https://doi.org/10.5194/acp-14-3497-2014>, 2014.
- Nguyen, T. B., Bates, K. H., Crounse, J. D., Schwantes, R. H., Zhang, X., Kjaergaard, H. G., Surratt, J. D., Lin, P., Laskin, A., Seinfeld, J. H., and Wennberg, P. O.: Mechanism of the hydroxyl radical oxidation of methacryloyl peroxyxynitrate (MPAN) and its pathway toward secondary organic aerosol formation in the atmosphere, *Phys. Chem. Chem. Phys.*, 17, 17914–17926, <https://doi.org/10.1039/C5CP02001H>, 2015.
- Pandis, S. N., Paulson, S. E., Seinfeld, J. H., and Flagan, R. C.: Aerosol formation in the photooxidation of isoprene and β -pinene, *Atmos. Environ.-A Gen.*, 25, 997–1008, [https://doi.org/10.1016/0960-1686\(91\)90141-S](https://doi.org/10.1016/0960-1686(91)90141-S), 1991.
- Paulot, F., Crounse, J. D., Kjaergaard, H. G., Kürten, A., Clair, J. M. S., Seinfeld, J. H., and Wennberg, P. O.: Unexpected epoxide formation in the gas-phase photooxidation of isoprene, *Science*, 325, 730–733, <https://doi.org/10.1126/science.1172910>, 2009.
- Pope III, C. A. and Dockery, D. W.: Health effects of fine particulate air pollution: lines that connect, *J. Air Waste Manage.*, 56, 709–742, 2006.
- Pöschl, U., Martin, S. T., Sinha, B., Chen, Q., Gunthe, S. S., Huffman, J. A., Borrmann, S., Farmer, D. K., Garland, R. M., Helas, G., Jimenez, J. L., King, S. M., Manzi, A., Mikhailov, E., Pauliquevis, T., Petters, M. D., Prenni, A. J., Roldin, P., Rose, D., Schneider, J., Su, H., Zorn, S. R., Artaxo, P., and Andreae, M. O.: Rainforest aerosols as biogenic nuclei of clouds and precipitation in the Amazon, *Science*, 329, 1513–1516, <https://doi.org/10.1126/science.1191056>, 2010.
- Ramanathan, V., Crutzen, P., Kiehl, J., and Rosenfeld, D.: Aerosols, climate, and the hydrological cycle, *Science*, 294, 2119–2124, 2001.
- Riedel, T. P., Lin, Y.-H., Zhang, Z., Chu, K., Thornton, J. A., Vizuete, W., Gold, A., and Surratt, J. D.: Constraining condensed-phase formation kinetics of secondary organic aerosol components from isoprene epoxydiols, *Atmos. Chem. Phys.*, 16, 1245–1254, <https://doi.org/10.5194/acp-16-1245-2016>, 2016.
- Riva, M., Bell, D. M., Hansen, A.-M. K., Drozd, G. T., Zhang, Z., Gold, A., Imre, D., Surratt, J. D., Glasius, M., and Zelenyuk, A.: Effect of organic coatings, humidity and aerosol acidity on multiphase chemistry of isoprene epoxydiols, *Environ. Sci. Technol.*, 50, 5580–5588, <https://doi.org/10.1021/acs.est.5b06050>, 2016a.
- Riva, M., Budisulistiorini, S. H., Chen, Y., Zhang, Z., D'Ambro, E. L., Zhang, X., Gold, A., Turpin, B. J., Thornton, J. A., Canagaratna, M. R., and Surratt, J. D.: Chemical characterization of secondary organic aerosol from oxidation of isoprene hydroxyhydroperoxides, *Environ. Sci. Technol.*, 50, 9889–9899, <https://doi.org/10.1021/acs.est.6b02511>, 2016b.
- Robinson, N. H., Hamilton, J. F., Allan, J. D., Langford, B., Oram, D. E., Chen, Q., Docherty, K., Farmer, D. K., Jimenez, J. L., Ward, M. W., Hewitt, C. N., Barley, M. H., Jenkin, M. E., Rickard, A. R., Martin, S. T., McFiggans, G., and Coe, H.: Evidence for a significant proportion of Secondary Organic Aerosol from isoprene above a maritime tropical forest, *Atmos. Chem. Phys.*, 11, 1039–1050, <https://doi.org/10.5194/acp-11-1039-2011>, 2011.
- Rohrer, F., Lu, K., Hofzumahaus, A., Bohn, B., Brauers, T., Chang, C.-C., Fuchs, H., Haseler, R., Holland, F., Hu, M., Kita, K., Kondo, Y., Li, X., Lou, S., Oebel, A., Shao, M., Zeng, L., Zhu, T., Zhang, Y., and Wahner, A.: Maximum efficiency in the hydroxyl-radical-based self-cleansing of the troposphere, *Nat. Geosci.*, 7, 559–563, <https://doi.org/10.1038/ngeo2199>, 2014.
- Romer, P. S., Duffey, K. C., Wooldridge, P. J., Allen, H. M., Ayres, B. R., Brown, S. S., Brune, W. H., Crounse, J. D., de Gouw, J., Draper, D. C., Feiner, P. A., Fry, J. L., Goldstein, A. H., Koss, A., Misztal, P. K., Nguyen, T. B., Olson, K., Teng, A. P., Wennberg, P. O., Wild, R. J., Zhang, L., and Cohen, R. C.: The lifetime of nitrogen oxides in an isoprene-dominated forest, *Atmos. Chem. Phys.*, 16, 7623–7637, <https://doi.org/10.5194/acp-16-7623-2016>, 2016.
- Rummel, U., Ammann, C., Kirkman, G. A., Moura, M. A. L., Foken, T., Andreae, M. O., and Meixner, F. X.: Seasonal variation of ozone deposition to a tropical rain forest in southwest Amazonia, *Atmos. Chem. Phys.*, 7, 5415–5435, <https://doi.org/10.5194/acp-7-5415-2007>, 2007.

- Schmid, B., Tomlinson, J. M., Hubbe, J. M., Comstock, J. M., Mei, F., Chand, D., Pekour, M. S., Kluzek, C. D., Andrews, E., Biraud, S. C., and McFarquhar, G. M.: The DOE ARM aerial facility, *B. Am. Meteorol. Soc.*, 95, 723–742, <https://doi.org/10.1175/BAMS-D-13-00040.1>, 2014.
- Slowik, J. G., Brook, J., Chang, R. Y.-W., Evans, G. J., Hayden, K., Jeong, C.-H., Li, S.-M., Liggio, J., Liu, P. S. K., McGuire, M., Mihele, C., Sjostedt, S., Vlasenko, A., and Abbatt, J. P. D.: Photochemical processing of organic aerosol at nearby continental sites: contrast between urban plumes and regional aerosol, *Atmos. Chem. Phys.*, 11, 2991–3006, <https://doi.org/10.5194/acp-11-2991-2011>, 2011.
- St. Clair, J. M., Rivera-Rios, J. C., Crouse, J. D., Knap, H. C., Bates, K. H., Teng, A. P., Jørgensen, S., Kjaergaard, H. G., Keutsch, F. N., and Wennberg, P. O.: Kinetics and products of the reaction of the first-generation isoprene hydroxy hydroperoxide (ISOPOOH) with OH, *J. Phys. Chem. A*, 120, 1441–1451, <https://doi.org/10.1021/acs.jpca.5b06532>, 2015.
- Surratt, J. D., Murphy, S. M., Kroll, J. H., Ng, N. L., Hildebrandt, L., Sorooshian, A., Szmigielski, R., Vermeylen, R., Maenhaut, W., Claeys, M., Flagan, R. C., and Seinfeld, J. H.: Chemical composition of secondary organic aerosol formed from the photooxidation of isoprene, *J. Phys. Chem. A*, 110, 9665–9690, <https://doi.org/10.1021/jp061734m>, 2006.
- Surratt, J. D., Lewandowski, M., Offenberg, J. H., Jaoui, M., Kleindienst, T. E., Edney, E. O., and Seinfeld, J. H.: Effect of acidity on secondary organic aerosol formation from isoprene, *Environ. Sci. Technol.*, 41, 5363–5369, <https://doi.org/10.1021/es0704176>, 2007a.
- Surratt, J. D., Kroll, J. H., Kleindienst, T. E., Edney, E. O., Claeys, M., Sorooshian, A., Ng, N. L., Offenberg, J. H., Lewandowski, M., Jaoui, M., Flagan, R. C., and Seinfeld, J. H.: Evidence for organosulfates in secondary organic aerosol, *Environ. Sci. Technol.*, 41, 517–527, <https://doi.org/10.1021/es062081q>, 2007b.
- Surratt, J. D., Chan, A. W., Eddingsaas, N. C., Chan, M., Loza, C. L., Kwan, A. J., Hersey, S. P., Flagan, R. C., Wennberg, P. O., and Seinfeld, J. H.: Reactive intermediates revealed in secondary organic aerosol formation from isoprene, *P. Natl. Acad. Sci. USA*, 107, 6640–6645, <https://doi.org/10.1073/pnas.0911114107>, 2010.
- Torres, A. and Buchan, H.: Tropospheric nitric oxide measurements over the Amazon Basin, *J. Geophys. Res.-Atmos.*, 93, 1396–1406, <https://doi.org/10.1029/JD093iD02p01396>, 1988.
- Trebs, I., Mayol-Bracero, O. L., Pauliquevis, T., Kuhn, U., Sander, R., Ganzeveld, L., Meixner, F. X., Kesselmeier, J., Artaxo, P., and Andreae, M. O.: Impact of the Manaus urban plume on trace gas mixing ratios near the surface in the Amazon Basin: Implications for the NO-NO₂-O₃ photostationary state and peroxy radical levels, *J. Geophys. Res.-Atmos.*, 117, D05307, <https://doi.org/10.1029/2011JD016386>, 2012.
- Ulbrich, I. M., Canagaratna, M. R., Zhang, Q., Worsnop, D. R., and Jimenez, J. L.: Interpretation of organic components from Positive Matrix Factorization of aerosol mass spectrometric data, *Atmos. Chem. Phys.*, 9, 2891–2918, <https://doi.org/10.5194/acp-9-2891-2009>, 2009.
- Valin, L., Russell, A., and Cohen, R.: Variations of OH radical in an urban plume inferred from NO₂ column measurements, *Geophys. Res. Lett.*, 40, 1856–1860, <https://doi.org/10.1002/grl.50267>, 2013.
- Volkamer, R., San Martini, F., Molina, L. T., Salcedo, D., Jimenez, J. L., and Molina, M. J.: A missing sink for gas-phase glyoxal in Mexico City: Formation of secondary organic aerosol, *Geophys. Res. Lett.*, 34, L19807, <https://doi.org/10.1029/2007GL030752>, 2007.
- Wang, W., Kourtchev, I., Graham, B., Cafmeyer, J., Maenhaut, W., and Claeys, M.: Characterization of oxygenated derivatives of isoprene related to 2-methyltetrols in Amazonian aerosols using trimethylsilylation and gas chromatography/ion trap mass spectrometry, *Rapid. Commun. Mass Sp.*, 19, 1343–1351, <https://doi.org/10.1002/rcm.1940>, 2005.
- Wennberg, P.: Let's abandon the “high NO_x” and “low NO_x” terminology, *IGAC news*, 50, 3–4, 2013.
- Worton, D. R., Surratt, J. D., LaFranchi, B. W., Chan, A. W. H., Zhao, Y., Weber, R. J., Park, J.-H., Gilman, J. B., de Gouw, J., Park, C., Schade, G., Beaver, M., Clair, J. M. S., Crouse, J., Wennberg, P., Wolfe, G. M., Harrold, S., Thornton, J. A., Farmer, D. K., Docherty, K. S., Cubison, M. J., Jimenez, J.-L., Frossard, A. A., Russell, L. M., Kristensen, K., Glasius, M., Mao, J., Ren, X., Brune, W., Browne, E. C., Pusede, S. E., Cohen, R. C., Seinfeld, J. H., and Goldstein, A. H.: Observational insights into aerosol formation from isoprene, *Environ. Sci. Technol.*, 47, 11403–11413, <https://doi.org/10.1021/es4011064>, 2013.
- Xu, L., Guo, H., Boyd, C. M., Klein, M., Bougiatioti, A., Cerully, K. M., Hite, J. R., Isaacman-VanWertz, G., Kreisberg, N. M., Knote, C., Olson, K., Koss, A., Goldstein, A. H., Hering, S. V., de Gouw, J., Baumann, K., Lee, S.-H., Nenes, A., Weber, R. J., and Ng, N. L.: Effects of anthropogenic emissions on aerosol formation from isoprene and monoterpenes in the southeastern United States, *P. Natl. Acad. Sci. USA*, 112, 37–42, <https://doi.org/10.1073/pnas.1417609112>, 2015.
- Zhang, Q., Jimenez, J. L., Canagaratna, M. R., Allan, J. D., Coe, H., Ulbrich, I., Alfarra, M. R., Takami, A., Middlebrook, A. M., Sun, Y. L., Dzepina, K., Dunlea, E., Docherty, K., DeCarlo, P. F., Salcedo, D., Onasch, T., Jayne, J. T., Miyoshi, T., Shimojo, A., Hatakeyama, S., Takegawa, N., Kondo, Y., Schneider, J., Drewnick, F., Borrmann, S., Weimer, S., Demerjian, K., Williams, P., Bower, K., Bahreini, R., Cottrell, L., Griffin, R. J., Rautiainen, J., Sun, J. Y., Zhang, Y. M., and Worsnop, D. R.: Ubiquity and dominance of oxygenated species in organic aerosols in anthropogenically-influenced Northern Hemisphere midlatitudes, *Geophys. Res. Lett.*, 34, L13801, <https://doi.org/10.1029/2007GL029979>, 2007.